Biomaterials xxx (2014) 1–15

Contents lists available at ScienceDirect

Biomaterials

journal homepage: www.elsevier.com/locate/biomaterials

Leading opinion

A safe-by-design approach to the development of gold nanoboxes as carriers for internalization into cancer cells

Dania Movia [a], Valerie Gerard [a,c], Ciaran Manus Maguire [b], Namrata Jain [b], Alan P. Bell [d], Valeria Nicolosi [a,c,e], Tiina O'Neill [f], Dimitri Scholz [f], Yurii Gun'ko [a,c], Yuri Volkov [a,b], Adriele Prina-Mello [a,b,*]

[a] Centre for Research on Adaptive Nanostructures and Nanodevices (CRANN), Trinity College Dublin, Dublin, Ireland
[b] School of Medicine, Trinity College Dublin, Dublin, Ireland
[c] School of Chemistry, Trinity College Dublin, Dublin, Ireland
[d] Advanced Microscopy Laboratory, Trinity College Dublin, Dublin, Ireland
[e] School of Physics, Trinity College Dublin, Dublin, Ireland
[f] UCD Conway Institute of Biomolecular and Biomedical Research, University College Dublin, Belfield, D4 Dublin, Ireland

ARTICLE INFO

Article history:
Received 26 November 2013
Accepted 19 December 2013
Available online xxx

Keywords:
Gold nanoboxes
Lung cancer barrier
High content screening and He-ion microscopy
Safe-by-design
Tiered approach
Three-dimensional culture

ABSTRACT

Gold nanomaterials are currently raising a significant interest for human welfare in the field of clinical diagnosis, therapeutics for chronic pathologies, as well as of many other biomedical applications. In particular, gold nanomaterials are becoming a promising technology for developing novel approaches and treatments against widespread societal diseases such as cancer. In this study, we investigated the potential of proprietary gold nanoboxes (AuNBs) as carriers for their perspective translation into multifunctional, pre-clinical nano-enabled systems for personalized medicine approaches against lung cancer. A safe-by-design, tiered approach, with systematic tests conducted in the early phases on uncoated AuNBs and more focused testing on the coated, drug-loaded nanomaterial toward the end, was adopted. Our results showed that uncoated AuNBs could effectively penetrate into human lung adenocarcinoma (A549) cells when in simple (mono-cultures) or complex (co- and three-dimensional-cultures) *in vitro* microenvironments mimicking the alveolar region of human lungs. Uncoated AuNBs were biologically inert in A549 cells and demonstrated signs of biodegradability. Concurrently, preliminary data revealed that coated, drug-loaded AuNBs could efficiently deliver a chemotherapeutic agent to A549 cells, corroborating the hypothesis that AuNBs could be used in the future for the development of personalized nano-enabled systems for lung cancer treatment.

1. Introduction

Gold nanomaterials have been used in biomedical applications since the discovery of gold colloids more than three centuries ago [1] and, as stated by Dreaden *at al.* in a recently published review [2], "a new 'Golden Age' of biomedical nanotechnology is upon us". The recent, growing interest in gold nanomaterials arises from their unique combination of photophysical properties (such as large and tuneable light extinction, localized surface plasmon resonance (LSPR), surface-enhanced Raman scattering (SERS) and efficient thermal ablation, to name a few), which can find exploitation in a wide range of diagnostic, biomedical and therapeutic applications.

To date, nanometer-sized gold materials are employed in the healthcare market as part of *in vitro* diagnostic devices [3] (e.g., First Response® pregnancy test – Carter-Wallace; Duopath® Verotoxins – Merck Millipore; ImmunoCAP® Rapid test – Phadia, Inc; and Verigene® platform – Nanospheres [4]) allowing the detection of biologically relevant molecules from complex fluids, such as blood plasma, with unprecedented limits of detection. In addition, the use of gold nanomaterials is currently under clinical evaluation for the treatment of solid tumours by laser-induced thermal ablation (e.g. the AuroLase® Therapy [5] by Auroshell™ particles [6] – Nanospectra Biosciences, at present in phase I of clinical trials [4,7]) or by delivering anti-cancer agents (e.g. Aurimmune – CytImmune Sciences, currently in phase II of clinical trials [4,7]). Finally, gold nanomaterials (including nanoparticles, nanoclusters, nanorods,

* Corresponding author. Centre for Research on Adaptive Nanostructures and Nanodevices (CRANN), Trinity College Dublin, College Green, D2 Dublin, Ireland. Tel.: +353 1 8963259, +353 1 8963087; fax: +353 1 8963037.
E-mail address: prinamea@tcd.ie (A. Prina-Mello).

0142-9612/$ – see front matter © 2013 Elsevier Ltd. All rights reserved.
http://dx.doi.org/10.1016/j.biomaterials.2013.12.057

nanoshells and nanoporous surfaces) are employed in biomedical research [1,8] as *in vitro*/*in vivo* imaging tools [2,9], optical sensors [10,11], photothermal therapeutics [12] and drug delivery systems [2,13,14]. By exploiting the high affinity of gold surfaces for thiols, gold nanomaterials provide in fact optimal chemical reactivity conditions for functionalization of their surface with biologically active moieties (e.g. targeting and therapeutic molecules) [1]. In the near future, safely applicable (e.g. non-toxic) gold nanotechnology-products are expected to improve patients' treatment through a more adaptive and personalized approach to medicine [15], where a single construct can accumulate in the site of interest (targeting component) while allowing simultaneous diagnosis of the disease, tracking of the drug delivery (imaging component) and selective drug release to the target cells/tissue (therapy component). The personalized treatment approach through gold nanomaterials will therefore offer the opportunity to decrease the adverse side-effects of drugs, focussing the medical efforts at the target tissue/organ level [16].

The aim of our present experimental study was to evaluate the biological interactions of uncoated gold nanoboxes [17] (AuNBs) with *in vitro* models representative of the human alveolar barrier, thus defining their potential as candidates for perspective functionalization and translation into pre-clinical nano-enabled chemotherapeutic agents for the targeted and personalized treatment of lung cancer. AuNBs, which are hollow nanostructures in the shape of triangular prisms, were selected as nanoprisms are known to show a much higher degree of enhancement of the plasmon resonance energy than nanospheres [18], finding application, for example, in Surface Enhanced Fluorescence (SEF) and Surface Enhanced Raman Spectroscopy (SERS) and opening up the opportunity of using AuNBs as imaging component of a perspective nano-enabled personalized treatment against lung cancer. Worldwide, lung cancer is one of the leading causes of cancer-related mortality, with more than 157,000 deaths only in 2010 [19,20]. The survival rate of patients with lung cancer is poor, with less than 15% of patients surviving 5 years after diagnosis [21]. Lung cancer is also the third most common cancer in Ireland, accounting for 13.9% of cancers diagnosed in men and 9.4% in women during the 1994–2008 period [21]. The statistical data on the survival rate of lung cancer patients clearly evidence the current lack of effective treatments to cure lung cancer [22] and the pressing need of developing new therapeutic approaches, such as personalised nano-enabled treatments, against this disease.

In order to achieve our aim, a cross-disciplinary, three-tiered approach was used (Fig. 1). In Tier 1 the internalization of two types of uncoated AuNBs (differing from each other in size, ranging from 30 to 70 nm ca.) was assessed in *ín vitro* mono-, co- and three-dimensional (3D)-culture models of human lung adenocarcinoma (A549) cells, thus allowing an evaluation of their capability as carriers to enter into the cancer cells. The mechanism and time-dependence of cell internalization, the cytotoxicity and the biodegradation of uncoated AuNBs were also determined for assessing the safety of these nanostructures once they have entered the cells surrounding the targeted tumour tissue. Despite the fact that the Au nanoparticles with diameter above 2 nm are generally considered inert and non-toxic [23–25], dispersions of gold nanomaterials can in fact induce cytotoxicity [2,24]. Such toxicity can rise from residual chemicals of the synthesis process [23,26–28], free small molecules and metal ions present in the solution [29] or from the degradation of the gold core [23]. In Tier 2 and 3, through a safe-by-design approach [16], the long-term biocompatibility provided by a gelatine coating [30] was combined with the targeting of cancerous cells over-expressing folic acid (FA) receptors with the aim of assessing *in vitro* the ability of AuNBs to deliver a chemotherapeutic agent, namely Paclitaxel, following purpose-specific functionalization.

Our results demonstrated that uncoated AuNBs were internalised by A549 cells in mono-, co- and 3D-cultures. Although significant AuNBs internalization was achieved after 5–7 h exposure, AuNBs showed to be biologically safe in A549 cells up to 24 h. Concurrently, preliminary *in vitro* data suggested that AuNBs could indeed be a suitable carrier for the delivery of a chemotherapeutic agent following purpose-specific functionalization, thus ultimately advocating for further pre-clinical research on AuNBs as candidate for nano-enabled targeted treatment of lung cancer.

2. Materials and methods

Chemicals and solvents were purchased from commercial sources (Sigma–Aldrich, Fisher Scientific, Invitrogen and Calbiochem) and used as provided, unless otherwise specified in the manuscript.

For clarity purposes, uncoated AuNBs tested in Tier 1 will be referred to as $AuNB_1$ and $AuNB_2$, gelatine-coated AuNBs used in Tier 2 as $AuNB_3$, and, in Tier 3, gelatine-coated Paclitaxel-loaded AuNBs and gelatine-coated Paclitaxel-loaded AuNBs to which FA was conjugated will be indicated as $AuNB_4$ and $AuNB_5$, respectively (Fig. 2).

2.1. Synthesis of uncoated AuNBs ($AuNB_1$ and $AuNB_2$)

AuNBs in two different size ranges were synthetized according to previously published protocols [17,31]. A complete description of the synthetic procedure is reported in the Supporting Data.

2.2. Physico-chemical characterization of uncoated AuNBs

Table 1 reports the main properties of uncoated AuNBs ($AuNB_1$ and $AuNB_2$). Uncoated AuNBs were characterised by transmission electron microscopy (TEM), He-ion microscopy (HIM), Nanoparticles Tracking Analysis (NTA) and pH measurements, as described below.

2.2.1. Transmission electron microscopy (TEM) of AuNBs

The TEM specimens were prepared on 200-mesh Cu lacey carbon grids by drop-casting and were visualized under a FEI Titan Transmission Electron Microscope (FEI,

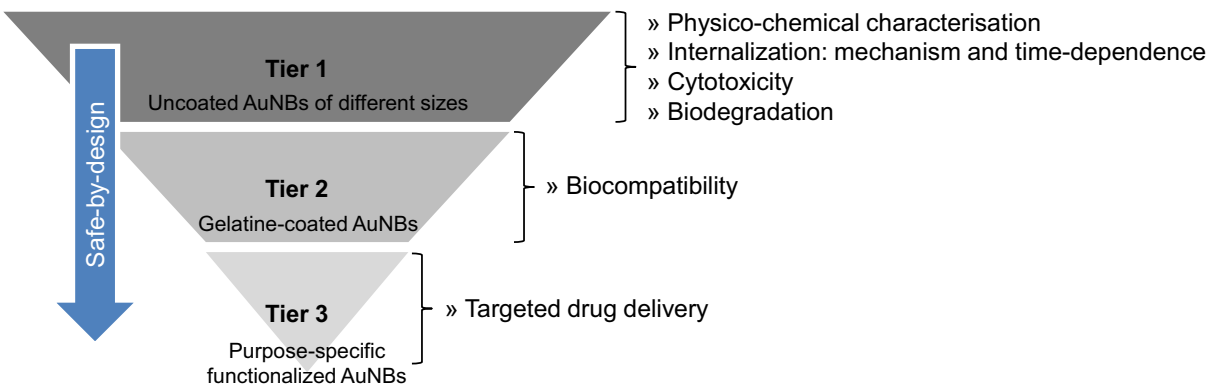

Fig. 1. Schematic of the safe-by-design, tiered approach used in this study to design a non-toxic nano-enabled carrier for therapeutic applications.

Please cite this article in press as: Movia D, et al., A safe-by-design approach to the development of gold nanoboxes as carriers for internalization into cancer cells, Biomaterials (2014), http://dx.doi.org/10.1016/j.biomaterials.2013.12.057

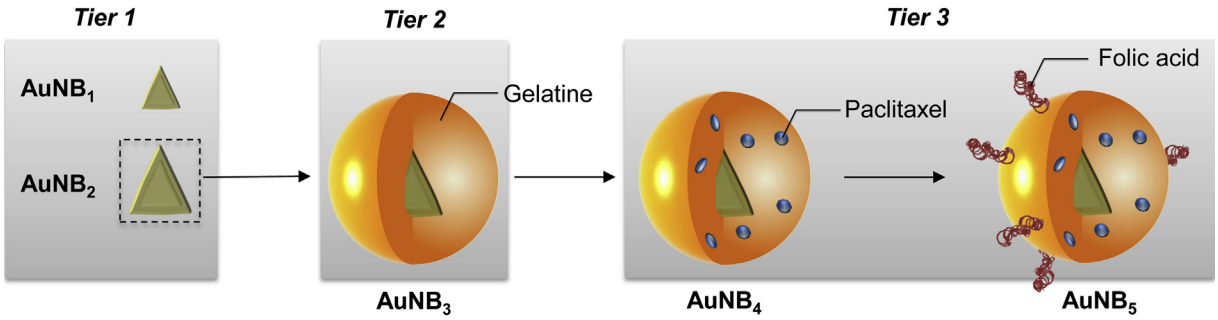

Fig. 2. Schematic of the structure of uncoated ($AuNB_1$ and $AuNB_2$) and functionalized ($AuNB_3$, $AuNB_4$ and $AuNB_5$) AuNBs.

Oregon, USA) operating at 300 kV. Size distributions graphs based on TEM images are reported in Fig. S1 in the Supplementary Data. The average size values (Table 1) were calculated on a sample population of 100 AuNBs.

2.2.2. He-ion microscopy (HIM)

AuNBs specimens were prepared on 200-mesh Cu lacey carbon grids or on silicon substrates by drop-casting, and imaged by a Zeiss Orion Plus He-ion microscope using an accelerating voltage of 30 kV. Samples were transferred into the chamber, which had undergone plasma clean overnight prior to loading samples, using a load lock. The working distance was 8 mm and a 10 μm aperture. The probe current was between 0.5 and 1.5 pA. Images were acquired by collecting the secondary electrons emitted by the interaction between the He-ion beam and the specimen with an Everhart-Thornley detector. The image signal was acquired in a 32 or 64 line integration to each contributing line of the image.

2.2.3. Nanoparticle tracking analysis (NTA) and pH measurements

Stock solutions of AuNBs were vortexed for 5 s and then diluted in DEPC treated ultrapure DI water at final concentration of 1.3×10^{-11} M. The dispersions were analysed *via* the NTA NS500 system (NanoSight, Amesbury, UK), thus determining hydrodynamic radius and zeta potential. Measurements were carried out at pH = 7 and room temperature six depth positions, recording two videos of 60 s at depth 1 and two videos of 30 s at each subsequent position and applying a voltage of 24 V. The validation of the protocol used in this study to perform the NTA measurements has been previously published [32]. pH was measured by a Russell RL060P portable pH meter (Thermo Electron Corporation, USA) coupled with a Pellon junction microelectrode (VWR, Ireland). All pH measurements were carried out under the same environmental conditions.

Based on the higher stability of the $AuNB_2$ aqueous solution (zeta potential = -57.4 ± 8.2 mV) and therefore shelf-life and applicability as compared to $AuNB_1$ dispersion, $AuNB_2$ were then brought forward in Tier 2 and Tier 3 for a proof-of-principle study on targeted anti-cancer drug delivery.

2.3. Synthesis of functionalized AuNBs ($AuNB_3$, $AuNB_4$ and $AuNB_5$)

In order to provide preliminary evidence on the ability of AuNBs to act as carrier for anti-cancer treatments, $AuNB_2$ were first coated with gelatine ($AuNB_3$), then loaded with Paclitaxel ($AuNB_4$) and finally functionalized with FA ($AuNB_5$) (Fig. 2). A detailed description of the synthetic protocol, adapted from a previously published work [33], is reported in the Supporting Data. Gelatine was introduced to increase the long-term biocompatibility of AuNBs [30] and to allow the loading of the chemotherapeutic agent (Paclitaxel) onto AuNBs surface. Attachment of FA to the AuNBs surface had the scope of increasing the targeting specificity of our nanomaterial [34], producing a targeted nanotechnology-based system that delivers the drug specifically to the cancer cells reducing the interactions with healthy tissues [35].

Table 1
Physico-chemical properties of AuNBs. With exception of pH data, all values are reported as mean ± standard deviation.

	Stock solutions		Final experimental conditions[a]	
	TEM size ($Ø_{TEM}$, nm)	pH (in water)	Hydrodynamic radius (in water, nm)	Zeta potential (mV)
$AuNB_1$	37 ± 6	6.6	90 ± 57	−23.4 ± 8.3
$AuNB_2$	62 ± 12	5.7	105 ± 38	−57.4 ± 8.2

[a] Hydrodynamic radius and zeta potential were measured at pH = 7 and AuNBs concentration equal to 1.3×10^{-11} M.

2.4. Cell culture

Human alveolar epithelial adenocarcinomic cells (A549 cell line) and human monocytic leukaemia cells (THP-1 cell line) were obtained from the American Tissue Culture Collection (ATCC, USA). A549 cells were cultured in Hams F12K media (supplemented with 2 nM L-glutamine, 1% penicillin/streptomycin and 10% foetal bovine serum (FBS)), while THP-1 cells were cultured in RPMI 1640 media (supplemented with 2 nM L-glutamine, 1% penicillin/streptomycin and 10% FBS). Cells were incubated at 37 °C and 5% CO_2. Mycoplasma and phenotypic responses were regularly checked for contamination as part of the laboratory GLP. The passage number was restricted between five and twelve. At 80% confluence, A549 cells were detached from T75 flask substrate with TryplE™ (Gibco, Invitrogen, Oregon, USA), centrifuged, counted using a Countess™ Automated Cell Counter (Invitrogen, Oregon, USA) and diluted in supplemented media at concentrations appropriate for each experimental protocol. When 60% confluence was reached, THP-1 cells were activated in a T25 flask with 30 ng/ml phorbol-12-myristate-13-acetate (PMA) (Sigma–Aldrich, USA) for 72 h to induce their differentiation into adherent macrophages and stop their natural proliferation. After 72 h THP-1 cells were washed and stained with 20 μM Cell Tracker™ Green CMFDA (Invitrogen, Oregon, USA) for 45 min at 37 °C and 5% CO_2 to allow their identification in co-culture models. THP-1 cells were then washed with fresh supplemented media, detached from flask substrate with TryplE™ (10 min, 37 °C), counted using a Countess™ Automated Cell Counter (Invitrogen, Oregon, USA) and diluted in supplemented media at concentrations appropriate for each experiment.

2.4.1. Mono-culture models

A549 and PMA-activated THP-1 cells were plated in 4-well Millicell® EZ Slide (Millipore™, MA, USA) at a concentration of 5000 and 1000 cells/well, respectively (final volume: 500 μl/well). Cells were incubated for 24 h at 37 °C (5% CO_2) to allow cell attachment to the glass substrate. When cultured under inverted culture conditions, A549 cells mono-cultures grown on glass slides were placed on sterile glass-slide holders with the cells facing the bottom of the petri-dish and immersed into a dispersion of AuNBs in supplemented cell media.

2.4.2. Co-Culture models

To produce a co-culture representative of the cellular composition of alveoli in the human lungs, A549 and PMA-activated THP-1 cells were seeded in a ratio 9:1 [36]. The 9:1 ratio corresponds to the ratio between the total number of cells (230×10^9 cells) across the whole alveolar area, which are mainly epithelial cells, and the number of alveolar macrophages (22×10^9 cells) [37]. A549 cells (doubling time: 22 h) were plated in 4-well Millicell® EZ Slide at a concentration of 5000 cells/well and incubated for 24 h at 37 °C and 5% CO_2 to allow cell attachment. After 24 h, PMA-activated THP-1 cells were plated onto the A549 culture at a concentration of 1000 cells/well to achieve a 9:1 ratio (A549:THP-1 cells). Co-cultures were then incubated for 24 h at 37 °C and 5% CO_2 to allow THP-1 cells attachment. The adhesion of THP-1 cells on top of the epithelial cells was shown by confocal microscopy imaging (reported in Fig. S2 in the Supporting Data) at confirmation of the successful co-existence of the two cell types.

2.4.3. 3D-culture models

A549 cells were seeded onto layers (thickness around 1 mm) of Matrigel™ Basement Membrane Matrix or PuraMatrix™ Peptide Hydrogel (both from BD Biosciences, UK). Matrigel™ is a solubilized basement membrane preparation extracted from the Engelbreth-Holm-Swarm (EHS) mouse sarcoma, a tumour rich in extracellular matrix proteins; PuraMatrix™ is a synthetic matrix that is used to create defined 3D microenvironments for a variety of cell culture experiments. Briefly, Matrigel™ Basement Membrane Matrix was thawed by submerging the vial in ice in a 4 °C refrigerator overnight. The vial was then swirled to ensure that the matrix was evenly dispersed and, using cooled pipette tips and keeping the glass slides on ice, the Matrigel™ Basement Membrane Matrix was added to the surface of a 4-well Millicell® EZ slide following the Thick Gel Method described by the supplier. This

Please cite this article in press as: Movia D, et al., A safe-by-design approach to the development of gold nanoboxes as carriers for internalization into cancer cells, Biomaterials (2014), http://dx.doi.org/10.1016/j.biomaterials.2013.12.057

method is recommended by BD Biosciences to grow cells within a 3D matrix. Slides were incubated at 37 °C for 30 min prior cell seeding. For PuraMatrix™, the stock solution (1% w/v) was diluted to the working concentrations of 0.25% with sterile DI water. 250 μl of PuraMatrix™ dilutions were then added to the surface of a 4-well Millicell® EZ slide and gelation was promoted by carefully and slowly adding supplemented F12K medium to each well (500 μl/well). The glass slide was incubated at 37 °C for 1 h to complete the gelation of the hydrogel. After the hydrogel has assembled, the medium was changed twice over a period of 1 h to equilibrate the environment to physiological pH. A549 cells were carefully seeded at the top of the Matrigel™ or PuraMatrix™ layers at a concentration of 10^6 cells/ml (500 μl/well). Cell cultures were grown for 4 d and cell medium was changed every 3 d.

2.5. Cellular internalization of uncoated AuNBs – qualitative analysis

The internalization of uncoated AuNBs into cells was assessed in *in vitro* mono-, co- and three-dimensional (3D)-cultures. Such *in vitro* models were exposed to $AuNB_1$ and $AuNB_2$ at a concentration of 1.3×10^{-11} M for 24 h. After 24 h exposure, three washings with phosphate-buffered saline (PBS) were carried out in order to completely remove the unbound and not-internalized AuNBs. Successful internalization of the nanomaterials was assessed by confocal microscopy and TEM.

2.5.1. Confocal microscopy

After fixation with 4% paraformaldehyde (PFA) for 10 min at room temperature, mono-, co- and 3D-cultures were stained with Hoechst 33342 for nuclei and rhodamine phalloidin (Invitrogen, Oregon, USA) for F-actin. The slides were incubated at room temperature for 1 h in the dark, rinsed with PBS and mounted in transparent mounting medium (VECTASHIELD, Vector Laboratories Inc., CA, USA) prior to confocal microscopy analysis by a ZEISS 510 Meta confocal microscope equipped with a Zeiss LSM 5 software (Carl Zeiss, Germany). AuNBs were imaged in reflectance mode at $\lambda_{exc} = 561$ nm. Qualitative confocal imaging was carried out by acquiring a series of z-stack images. Surface rendering of z-stack images was carried out by the open-source software BioImageXD [38] in order to further elucidate the AuNBs internalization.

2.5.2. Transmission electron microscopy (TEM) of biological specimens

TEM images of ultrathin sections of A549 cells cultured as mono- and 3D-cultures and exposed to $AuNB_2$ were examined. After exposure to $AuNB_2$, A549 cells were fixed at room temperature in 2.5% glutaraldehyde (GA) in 0.1 M Sørensen's phosphate buffer (pH 7.4), rinsed with Sørensen's phosphate buffer and then post-fixed for 1 h in 1% osmium tetroxide in 0.1 M Sørensen's phosphate buffer. After dehydration at increasing concentrations of EtOH (from 30% up to 100%), the samples were immersed in an ethanol/Epon (1:1 vol/vol) mixture for 1 h before being transferred to pure Epon at 37 °C for 2 h. The polymerization was carried out at 60 °C for 24 h. For orientation purposes sections from each sample were cut at 1 μm, stained with toluidine blue, and examined by light microscopy (Nikon Eclipse TE300 epifluorescence microscope). From these survey sections areas of interest were identified and ultrathin sections of 80 nm, were obtained with a diamond knife using a Leica EM UC6 ultramicrotome (Leica, Germany). These sections were mounted on EM grids (300-mesh Cu grids) and stained with uranyl acetate and lead citrate before being examined with a TEM (FEI TECNAI Transmission Electron Microscope or FEI Titan Transmission Electron Microscope (FEI, Oregon, USA)).

2.5.3. Raman spectroscopy

The AuNBs internalized into A549 cells mono-cultures was also detected by Raman spectroscopy. A549 cells exposed to $AuNB_1$ and $AuNB_2$ as previously described were fixed with 2.5% GA in 0.1 M Sørensen's phosphate buffer (pH 7.3). Raman spectra were acquired using NTEGRA Spectra AFM-Raman microscope (NT-MDT, Russia) with a cobalt solid-state laser operating at a wavelength of 473 nm. All spectrums were recorded over the range of 2850–3800 cm^{-1} for 10 s, at 100% laser power, using a 100 × oil immersion objective and averaged across 5 scans per sample. Obtained spectra were analysed with baseline correction, smoothening and normalization using Renishaw WIRE software (Renishaw, Gloucestershire, UK).

2.6. Cellular internalization of uncoated AuNBs – time-dependence

Absorbance spectroscopy was used to quantify the amount of uncoated AuNBs internalized into A549 cells overtime. $AuNB_1$ and $AuNB_2$ have specific absorption peaks in the UV/Vis region (at 560 nm and 700 nm, respectively) that do not overlap with those of cellular components (see Fig. S3 in the Supporting Data). A549 cells mono-cultures were formed in 96-well plates (5000 cells/well) and were exposed to AuNBs (1.3×10^{-11} M) for 0, 1, 3, 5 and 7 h. At each time-point, cells were washed carefully with PBS to eliminate any unbound, not-internalized AuNBs; fixation then followed by incubation with 4% PFA for 10 min. Absorption at 560 nm and 700 nm was recorded by an Epoch microplate reader (Biotek, USA), calibrated against untreated cells and corrected by subtracting the optical aberration of the 96-well plastic plate at 540 nm. The absorption at 560 nm and 700 nm of known concentrations of AuNBs was also recorded at the same time, generating the calibration curve and allowing the quantification of the internalized AuNBs.

2.7. Cellular internalization of uncoated AuNBs – mechanism

To determine if uncoated AuNBs were internalized into cells by active or passive transport routes, A549 mono-cultures were exposed to $AuNB_1$ and $AuNB_2$ (1.3×10^{-11} M) for 24 h in the presence of inhibitors of the cellular energy-dependent mechanisms of uptake, *i.e.* at 4 °C or in the presence of sodium azide (NaN_3). For qualitative analysis, A549 cells were stained with Hoechst 33342 for nuclei and rhodamine phalloidin (Invitrogen, Oregon, USA) for F-actin for 1 h at room temperature in the dark. After washing with PBS, specimens were analysed by confocal microscopy, as previously described. For quantitative analysis, the intracellular accumulation of AuNBs was quantified by absorption spectroscopy by an Epoch microplate reader, as aforementioned.

2.8. Cytotoxicity of uncoated AuNBs

High Content Screening and Analysis (HCSA) and Enzyme-Linked Immunosorbent Assay (ELISA) assays were used to quantify the cytotoxic responses and cytokine secretion of A549 mono-cultures when exposed to uncoated AuNBs at four concentrations (2.1×10^{-12}, 5.3×10^{-12}, 1.1×10^{-11} and 1.3×10^{-11} M) for 24 h. A549 cells were plated in 96-well plates (Nunc Inc., USA) at a concentration of 5000 cells/well.

2.8.1. High content screening and analysis (HCSA)

Following exposure to uncoated AuNBs, a multiparametric cytotoxicity assay was performed using HCS reagent HitKit™ as per manufacturer's instructions (Thermo Fisher Scientific Inc., USA). Briefly, this kit enables to measure cell viability, cell membrane permeability and lysosomal mass/pH, which are toxicity-linked cellular markers. The experimental layout for the automated microscopic analysis, based on the In Cell Analyzer 1000, was composed of untreated cells (negative control or N/T), cells treated with uncoated AuNBs and cells exposed to doxorubicin (positive control or P/T) at a dose (200 μM) above the drug's IC_{50}. Images were acquired in a stereology configuration of ten randomly selected fields at 10× objective lens magnification using three detection channels with different excitation filters. The rate of cell viability and proliferation were assessed by the automated analysis of the nuclear count and morphology (DAPI filter); in parallel the fluorescent staining intensities reflecting cell permeability (FITC filter) and lysosomal mass/pH changes (TRITC filter) were also quantified for each individual cell present in the examined microscopic fields (IN Cell Investigator, GE Healthcare, UK).

2.8.2. Cytokines secretion

The secretion of the pro-inflammatory cytokine Interleukin-6 (IL-6) from A549 cells exposed to uncoated AuNBs was quantified by ELISA (Human IL-6 DuoSet ELISA kit, R&D Systems, Minneapolis, USA), according to the manufacturer's manual. The assay was carried out in triplicate on cells supernatant solutions. The optical density of each well at 450 nm was determined by means of an Epoch microplate reader (Biotek, USA), calibrated against standards and corrected by subtracting the optical aberration of the 96-well plastic plate at 540 nm.

2.9. Biodegradation of uncoated AuNBs

In order to investigate whether uncoated AuNBs were degraded by A549 cells, AuNBs were retrieved from A549 mono-cultures after exposure. Briefly, A549 cells were washed with PBS after 24, 48 or 72 h exposure to AuNBs in order to completely remove unbound, not-internalized AuNBs. Cells were then trypsinized, centrifuged and resuspended in DI water, thus causing cell swelling and osmotic burst. Cell bursting was facilitated by cell membrane damage caused by placing the water-saturated cells suspensions at −20 °C. Multiple cycles of centrifugation/resuspension were carried out to clean the AuNBs suspensions from the residual biological material. Collected AuNBs samples were then imaged by TEM and HIM, as previously described in the physico-chemical characterization section. In addressing topics of the biological sciences, HIM offers various advantages over conventional scanning electron microscopy (SEM) approaches, such as the ability to image uncoated, non-conductive samples without the deposition of a metal (or other conductive) overcoat [39,40], which can indeed destroy, reduce and/or completely mask details of the specimen surface. In this study, we deployed the high resolution imaging capabilities of HIM to image the adsorption of biological material onto AuNBs surface and the changes in particles morphology with unsurpassed image quality and detail. The hydrodynamic radius of the collected AuNBs was measured by NTA, as previously described.

2.10. Biocompatibility of gelatine-coated AuNBs ($AuNB_3$)

Following 24 h and 72 h exposure of A549 mono-cultures to $AuNB_3$ at a working concentration of 10^{-11} M, Trypan Blue exclusion assay was carried out. The experimental design included a negative control (untreated cells), a positive control (cells treated with 70% methanol for 30 min at 37 °C) and cells treated with $AuNB_2$ (10^{-11} M) as internal control. Each treatment was carried out in triplicate and experiments were carried out in duplicate. Live and dead cells were quantified by a Countess™ cell counter (Invitrogen, UK). The percentage (%) of live cells was then calculated as for Equation (1):

Please cite this article in press as: Movia D, et al., A safe-by-design approach to the development of gold nanoboxes as carriers for internalization into cancer cells, Biomaterials (2014), http://dx.doi.org/10.1016/j.biomaterials.2013.12.057

$$\%\text{live cells} = \frac{\text{live cells}}{(\text{live cells} + \text{dead cells})} \times 100 \quad (1)$$

2.11. Functionalized AuNBs ($AuNB_4$ and $AuNB_5$) for drug delivery – proof-of-principle

Trypan Blue exclusion assay was carried out after exposing A549 mono-cultures to $AuNB_4$ and $AuNB_5$ (10^{-11} M) for 24 and 72 h. The experimental design included a negative control (untreated cells), a positive control (cells treated with 70% methanol for 30 min at 37 °C) and cells treated with molecular Paclitaxel (0.03 mM) as term of comparison. Experimental protocol and quantification of the percentage of live cells was performed as described in the previous section.

2.12. Statistical analysis

Two-way analysis of variance (ANOVA) followed by a Bonferroni post-test analysis was carried out (Prism, Graph-Pad Software Inc., USA). A p value <0.05 was considered statistically significant. Unless differently stated in the manuscript, all data are presented as mean values ($n_{test} = 3$) ± standard deviation and normalized to the negative control.

3. Results

The three-tiered approach adopted in this study consisted of systematic tests conducted in Tier 1 on uncoated AuNBs and of more focused, preliminary testing on the coated, drug-loaded nanomaterials in Tier 2 and 3. Such approach finds his routes in the concept of safe-by-design nanomaterials, where efforts are focused on characterizing the physical, chemical and biological properties of the core material, followed by "layering" as a method to produce safe nano-enabled theranostics [16].

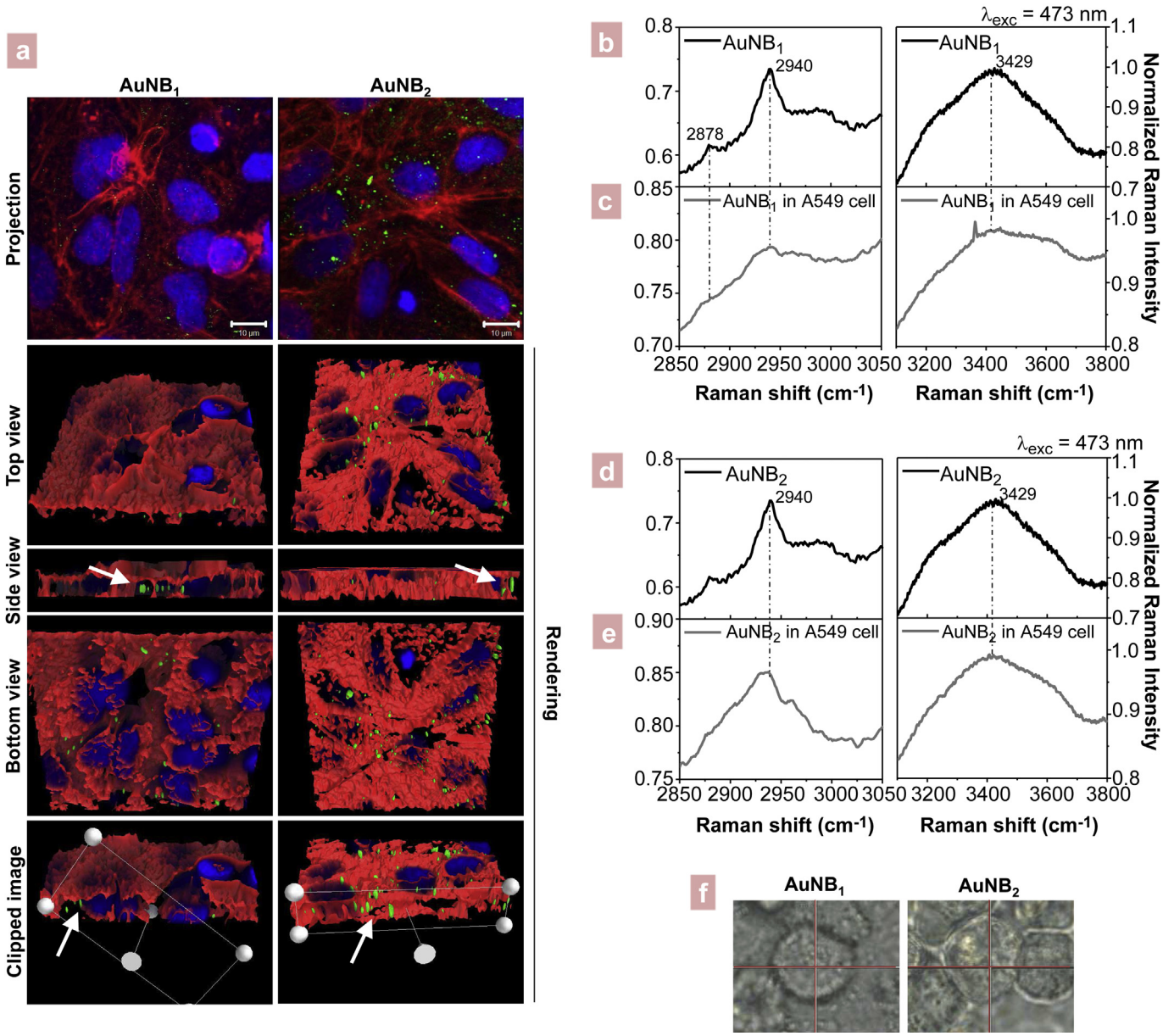

Fig. 3. Cellular internalization of uncoated AuNBs in mono-cultures of A549 cells after 24 h exposure. (a) Projections and rendered reconstructions of representative confocal micrographs of A549 cells exposed to AuNBs and stained with rhodamine phalloidin (F-actin, in red) and Hoechst 33342 (nuclei, in blue). AuNBs were imaged in confocal reflectance mode and are shown in green as pseudo-colour. The localization of AuNBs (indicated by arrows) in the cells cytoplasm is evident. Scale bars: 10 μm (63 × objective lens). (b, d) Raman spectra ($\lambda_{exc} = 473$ nm) of (b) $AuNB_1$ and (d) $AuNB_2$. The characteristic Raman bands of AuNBs (2878, 2940 and 3429 cm^{-1}) are clearly shown. (c, e) Raman spectra ($\lambda_{exc} = 473$ nm) of (c) $AuNB_1$ and (e) $AuNB_2$ internalized into A549 cells. (f) Brightfield images of A549 cells exposed to uncoated AuNBs. The red lines intersection show the point at which the Raman spectra reported in images c and e were collected, clearly evidencing that AuNBs were detectable in the area corresponding to the cells cytoplasm.

Please cite this article in press as: Movia D, et al., A safe-by-design approach to the development of gold nanoboxes as carriers for internalization into cancer cells, Biomaterials (2014), http://dx.doi.org/10.1016/j.biomaterials.2013.12.057

3.1. Tier 1

Uncoated AuNBs ($AuNB_1$ and $AuNB_2$) were synthetized by galvanic replacement reactions [17] [41], a method previously reported for the synthesis of bimetallic hollow nanostructures of a range of shapes and sizes. The AuNBs tested in Tier 1 were hollow nanoprisms with monodispersed sizes (height of the triangle: 37 ± 6 nm for $AuNB_1$ and 62 ± 12 nm for $AuNB_2$) and controlled thickness of the nanobox walls. The AuNBs aqueous dispersions produced were characterized by optimal colloidal stability (with zeta potential ranging from −20 to −60 mV ca.), thus allowing investigating the internalization of uncoated, non-functionalised AuNBs into the cells and any potential and/or unintended toxic effect that the gold core may induce as a consequence of cellular access.

3.1.1. Cellular internalization of uncoated AuNBs – qualitative analysis

In order to be one-step closer to *in vivo* complex scenarios, the effective internalization of uncoated AuNBs ($AuNB_1$ and $AuNB_2$) was assessed in *in vitro* mono-, co- and 3D-culture models representative of the human alveolar barrier. The exposure time was fixed at 24 h, which can be considered a pharmacological relevant time-point if compared to the infusion schedules used in clinical practice for chemotherapeutic agents such as Paclitaxel, ranging between 3 h and 24 h [42].

In mono-culture models, the internalization of uncoated AuNBs was assessed in A549 (Figs. 3 and 4) and THP-1 (see Fig. S4 in the Supporting Data) cells, as well as in a murine model of phagocytic cells (J774 cell line) (as described in the additional experimental section reported in the Supporting Data). While human and murine macrophage-like (THP-1 and J774) cells were used to represent the resident phagocytic cells in the alveoli, the A549 cell line was chosen as a physiologically relevant *in vitro* model of the *in vivo* non-small cell lung cancer (NSCLC) [43], the most prevalent form of lung cancer originating from epithelial cells, and therefore as an optimal cellular target for personalized medicine approaches. In addition A549 cells, as immortalised cell line, are considered one of the closest cell model to mimic alveolar epithelial type II cells (e.g. presenting membrane-bound inclusions, which resemble

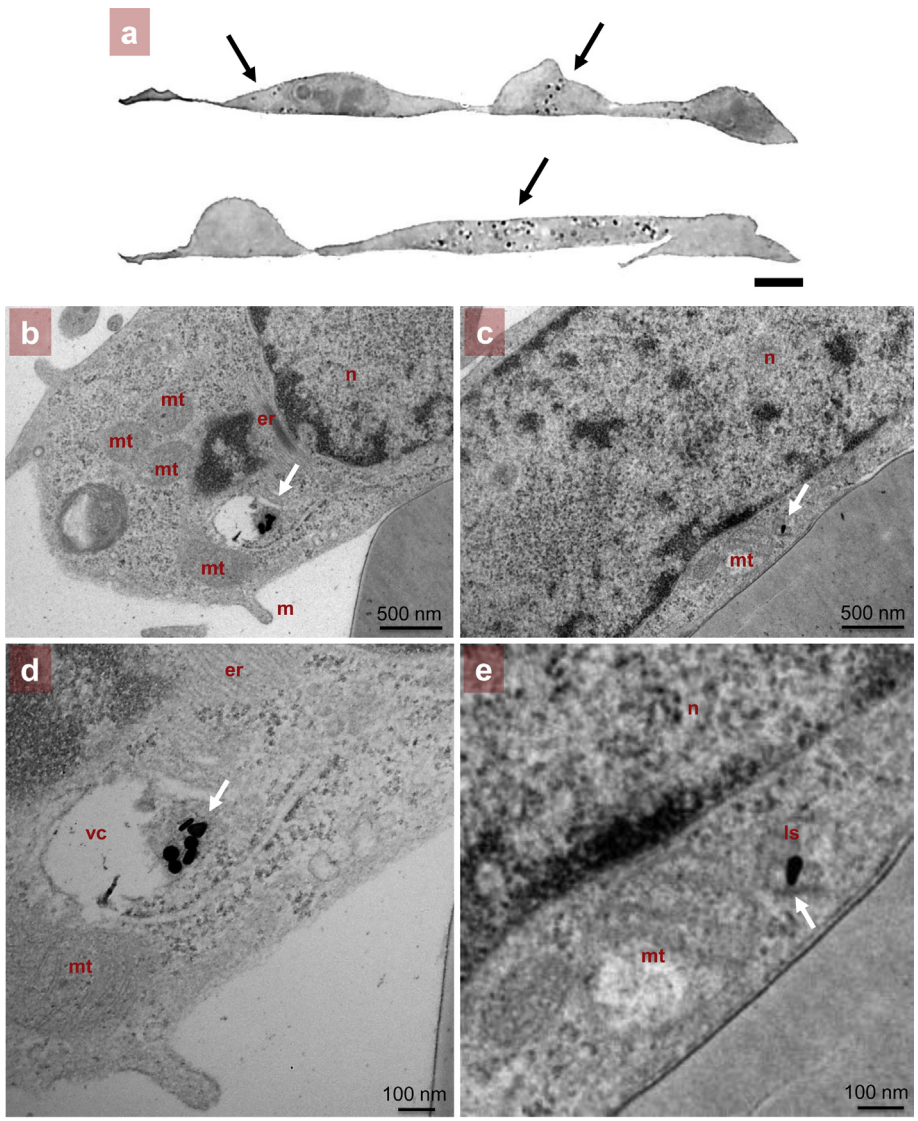

Fig. 4. Representative (a) light microscopy and (b–e) TEM images of ultrathin cross-sections (80 nm) of A549 cells exposed to $AuNB_2$ for 24 h. (a) The localisation of $AuNB_2$ (black dots indicated by arrows) into the cellular bodies is evident. Scale bar: 20 μm (100 × objective lens). (b–e) $AuNB_2$ (indicated by arrows) can be recognized by their geometrical shape and contrast as internalized in vacuoles and lysosomes. Images d and e are magnifications of images b and c, respectively. Abbreviations: er, endoplasmic reticulum; ls: lysosome; m: microvilli; mt: mitochondria; n: nucleus; vc: vacuole.

Please cite this article in press as: Movia D, et al., A safe-by-design approach to the development of gold nanoboxes as carriers for internalization into cancer cells, Biomaterials (2014), http://dx.doi.org/10.1016/j.biomaterials.2013.12.057

lamellar bodies of type II cells) [44] and, therefore, an appropriate epithelial alveolar cell model [45]. Finally, A549 cells have also proven to be a robust cell line/alveolar model for several previous nanomaterial-based studies [46–50].

Confocal microscopy images evidenced that uncoated AuNBs (imaged in reflectance mode) were effectively internalized into the A549, THP-1 and J774 cell mono-cultures (Fig. 3a, Fig. S4 and Fig. S6, respectively) and were found contained within the cells cytoplasm. Raman spectroscopy also confirmed that uncoated AuNBs were detectable in the areas corresponding to the A549 cells cytoplasm (Fig. 3c, e and 3f). In detail, the characteristic Raman signatures of AuNBs (bands at 2878, 2940 and 3429 cm^{-1}) (Fig. 3b and d) were detectable when A549 cells were exposed to AuNBs for 24 h (Fig. 3c and e). Such bands were unique of AuNBs and did not overlap with the Raman signals of the cell culture substrate (glass) or of the solutions in which cells were incubated and stored (Fig. S5 in the Supporting Data).

Further to this, light microscopy (Fig. 4a) and TEM (Fig. 4b–e) imaging of ultrathin cross-sections of A549 cells exposed to $AuNB_2$ and embedded in Epon resin showed that uncoated AuNBs (indicated by arrows in Fig. 4) were localized into the cellular bodies after 24 h. In detail, TEM images showed that $AuNB_2$ could be found stored in vacuoles and lysosomes of A549 cells (Fig. 4b–e), and suggested that $AuNB_2$ were trapped by cell membrane invagination (Fig. 4b and d).

Based on our experimental data showing that $AuNB_1$ and $AuNB_2$ were uptaken in macrophage-like cells (Fig. S4 and Fig. S6), we developed a co-culture system formed by A549 and THP-1 cells with the aim of mimicking the pivotal function of macrophages in the alveoli of the lung against inhaled particulate [51]; macrophages could therefore play a major role in the unexpected clearance of AuNBs before they reach the cellular target (*i.e.*, the lung adenocarcinoma cells). Confocal microscopy analysis of A549/THP-1 co-cultures demonstrated that $AuNB_1$ and $AuNB_2$ were internalized into A549 cells even when co-cultured with macrophage-like THP-1 cells (Fig. 5), and uncoated AuNBs could be detected in the cytoplasm of both cell types.

Finally, in 3D cell cultures, which were used to mimic more closely the native three-dimensional architecture and microenvironment of human lung adenocarcinomas [52], our results demonstrated that uncoated AuNBs were effectively internalized into A549 cells cultured onto hydrogels layers (Matrigel™ and PuraMatrix™). In particular, confocal analysis and TEM imaging showed that uncoated AuNBs were localised into the cytoplasm of cells grown onto PuraMatrix™ (Fig. 6a–b) or Matrigel™ (Fig. 6c). Interestingly, transmission electron micrographs evidenced that, in both 3D cell culture models, AuNBs were localised in lysosomes and characteristics cytoplasmic lamellar bodies (Fig. 6b and c).

3.1.2. Cellular internalization of uncoated AuNBs – time-dependence

Absorption measurements by a microplate reader were used with the purpose of defining the time needed to achieve significant internalization of uncoated AuNBs into A549 cell mono-cultures. In detail, the absorbance at 560 nm and 700 nm was measured to quantify the amount of internalized $AuNB_1$ and $AuNB_2$, respectively. Fig. 7a shows the concentration of AuNBs internalized into A549 cells at different time-points (0, 1, 3, 5 and 7 h). Significant internalization of $AuNB_1$ and $AuNB_2$ was achieved at 5 h and 7 h, respectively.

The influence of the *in vitro* environment on the time-dependent AuNBs internalization was also assessed. Confocal microscopy analysis of A549 cells cultured under inverted conditions and exposed to uncoated AuNBs showed that the internalization of these nanomaterials was nearly equal to zero after 24 h when A549 cells were cultured in these conditions (Fig. 7b). In agreement with previous studies on gold nanomaterials [53] and on other nanoparticulates [2,54], the time-dependent cellular internalization of

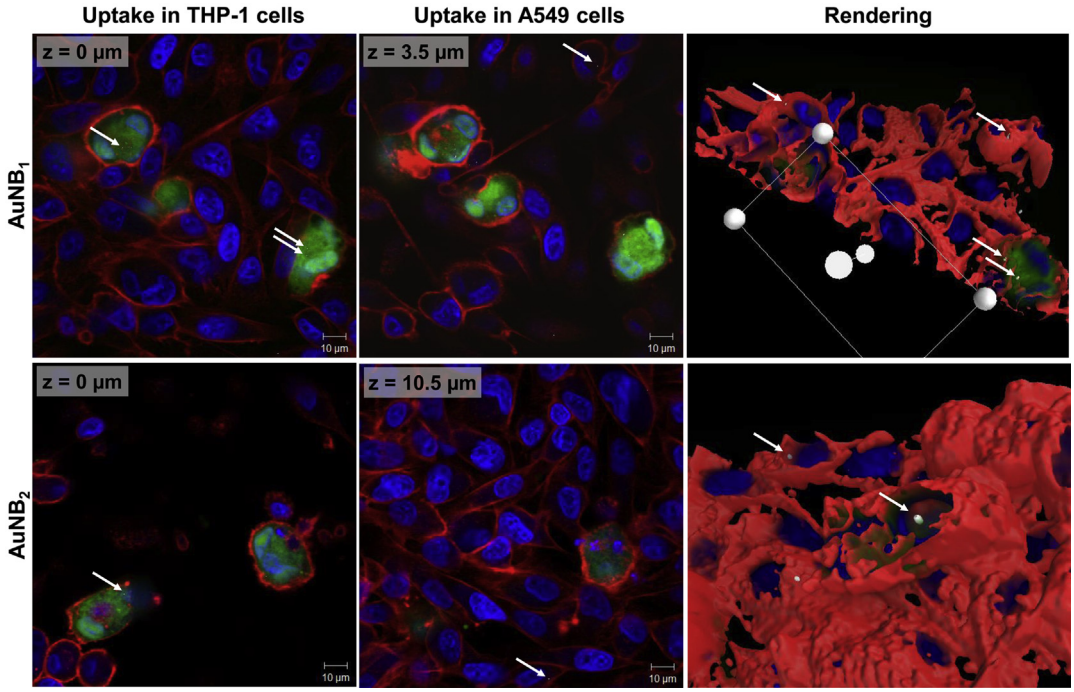

Fig. 5. Cellular internalization of uncoated AuNBs in co-cultures of A549 cells and macrophage-like THP-1 cells after 24 h exposure. Projections and rendered reconstructions of representative confocal microscopy images of AuNBs-treated co-cultures stained with Hoechst 33342 (nuclei, in blue) and rhodamine phalloidin (F-actin, in red). THP-1 cells were also stained with Cell Tracker™ Green CMFDA (in green). AuNBs were imaged in confocal reflectance mode and are shown in white as pseudo-colour. The localization of AuNBs in the cytoplasm of both cell types is highlighted by arrows. Scale bars: 10 µm (63 × objective lens).

Please cite this article in press as: Movia D, et al., A safe-by-design approach to the development of gold nanoboxes as carriers for internalization into cancer cells, Biomaterials (2014), http://dx.doi.org/10.1016/j.biomaterials.2013.12.057

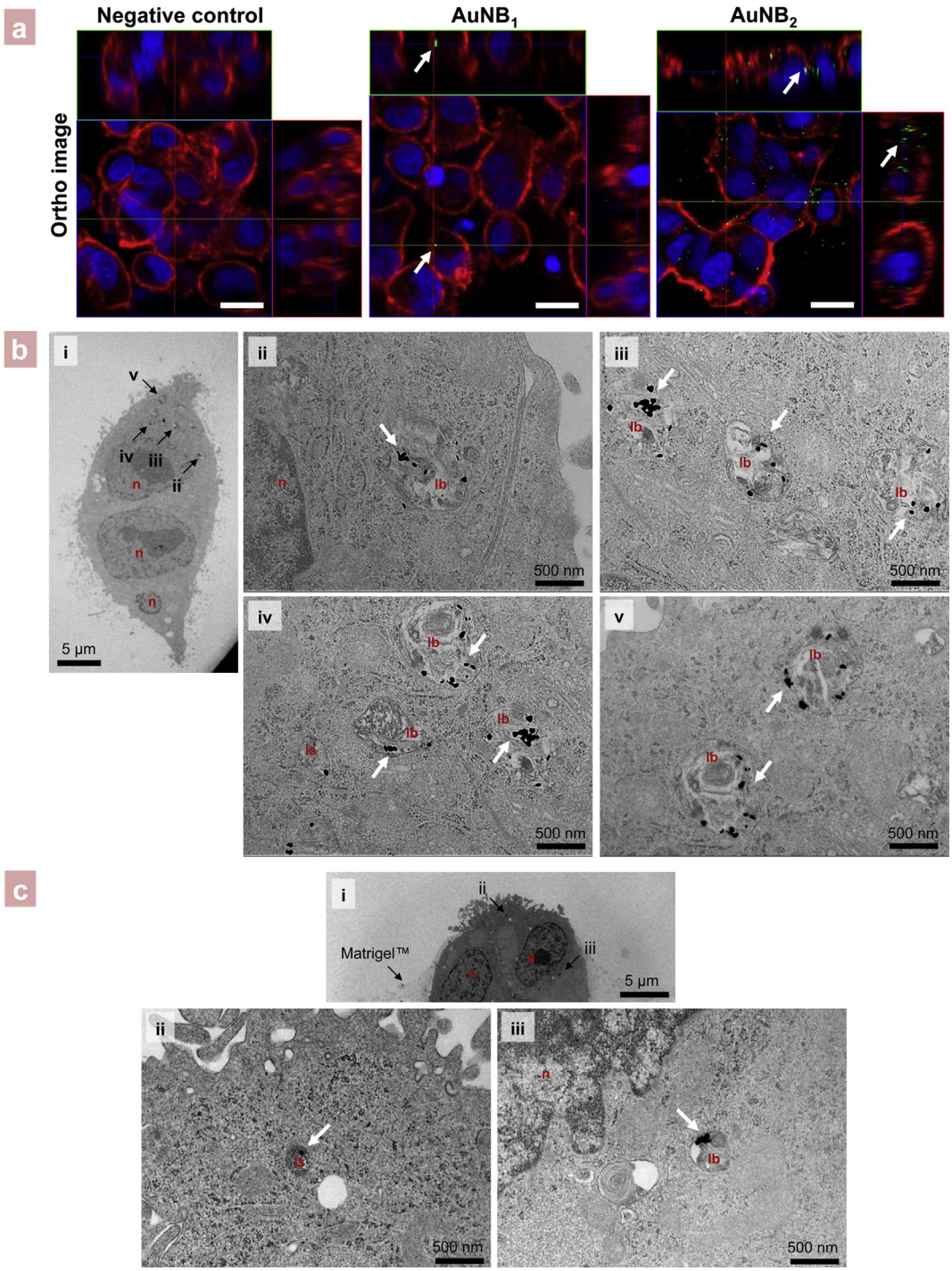

Fig. 6. Cellular internalization of uncoated AuNBs in 3D cell cultures grown onto (a, b) PuraMatrix™ (0.25%) or (c) Matrigel™. (a) Ortho-images of representative confocal micrographs of 3D cell cultures exposed to uncoated AuNBs and stained with rhodamine phalloidin (F-actin, in red) and Hoechst 33342 (nuclei, in blue). AuNBs were imaged in confocal reflectance mode and are shown in green as pseudo-colour. The localization of AuNBs (arrows) in the cells cytoplasm is evident. Scale bars: 10 μm (63 × objective lens). (b and c) TEM images of ultrathin cross-sections (80 nm) of 3D cell cultures grown onto (b) PuraMatrix™ (0.25%) or (c) Matrigel™ and exposed to $AuNB_2$ for 24 h $AuNB_2$ (indicated by white arrows) can be recognized by their geometrical shape and contrast as internalized in lysosomes and lamellar bodies. (b) Images ii-v are magnifications of image i. (c) Images ii and iii are magnifications of image i. Abbreviations: lb: lamellar bodies; ls: lysosome; n: nucleus.

uncoated AuNBs was therefore strongly influenced by their sedimentation rate.

3.1.3. *Cellular internalization of uncoated AuNBs – mechanism*

In order to define the mechanism of AuNBs internalization into lung adenocarcinoma cells, we investigated whether the cellular uptake of the uncoated AuNBs was mediated by an energy-dependent mechanism. Thus, A549 cells were exposed to $AuNB_1$ and $AuNB_2$ at 4 °C or in the presence of 0.1% sodium azide (NaN_3) for 24 h, and the AuNBs internalization was quantified by absorption spectroscopy. Results were then compared to the 37 °C experiment. A549 cells incubated at 4 °C did not exhibit any

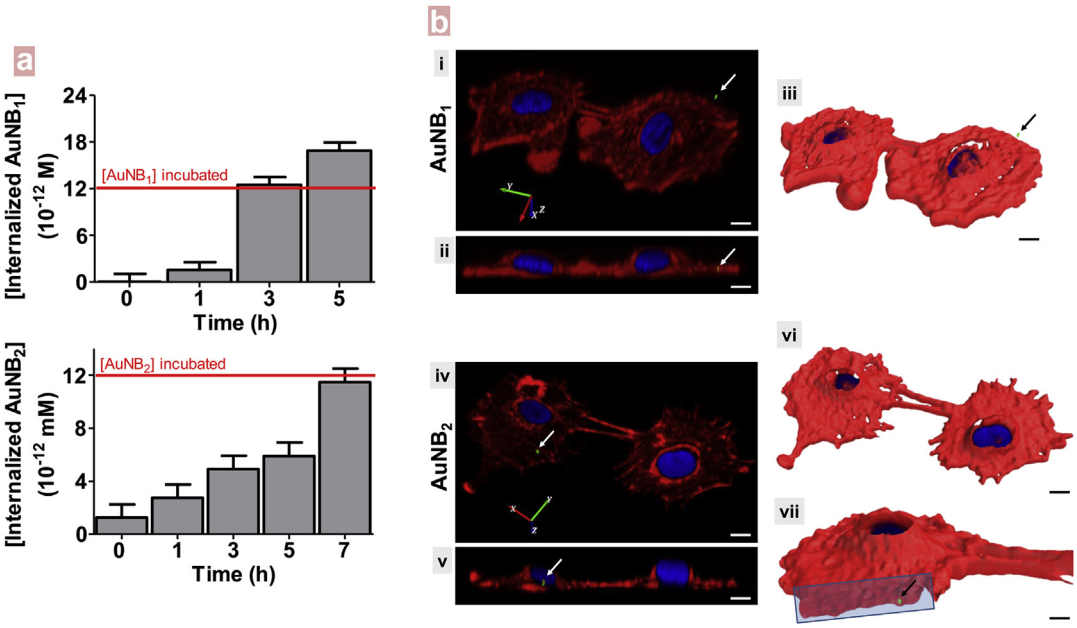

Fig. 7. (a) Internalization of uncoated AuNBs into A549 cells mono-cultures overtime. Concentration of AuNBs into cells after 0, 1, 3, 5 and 7 h, as quantified by absorption spectroscopy. Data are reported as mean ± standard deviation. (b) Internalization of (i-iii) $AuNB_1$ and (iv-vii) $AuNB_2$ into A549 cells cultured in an inverted configuration. Rendering of representative confocal images of AuNBs-treated cells, stained with rhodamine phalloidin (F-actin, in red) and Hoechst 33342 (nuclei, in blue). AuNBs (indicated by arrows) were imaged in confocal reflectance mode and are shown in green as pseudo-colour. (b: vii) Detail of image vi. The light-blue rectangle represents the clipping plane. The presence of a single uncoated AuNB inside the cell cytoplasm is highlighted. Scale bars: (i-vi) 10 μm, (vii) 5 μm (63× objective lens).

reduction in the AuNBs uptake as compared to the equivalent incubation at 37 °C (Fig. 8a and b). Moreover, blocking the active transport mechanism of the A549 cells by 0.1% NaN_3 treatment impeded only the uptake of $AuNB_1$ (Fig. 8a), leaving unaffected the $AuNB_2$ internalization grade (Fig. 8b). One important aspect to consider when inhibiting endocytosis is to leave unaffected the F-actin cytoskeleton of the cell, since reorganization of the actin filaments can impact on cellular uptake processes [55], leading to multiple effects occurring simultaneously. In our study, the F-actin filaments maintained their overall morphology and distribution when A549 cells were treated with NaN_3 (Fig. 8c), in accordance with previously published studies [56].

The hydrodynamic radius of the internalized AuNBs (Fig. 8d) appeared significantly increased when retrieved from A549 cells exposed for 24 h, as compared to reference, as-synthetized AuNBs (0 h). This indicated protein opsonisation, e.g. the adsorption of proteins such as serum albumin (which is richly in the cell culture media in the form of FBS) onto the surfaces of uncoated AuNBs [57,58]. These data were strongly supported by HIM imaging (Fig. 8e), showing that $AuNB_2$ retrieved from A549 cells mono-cultures after 24 h incubation were coated in biological material. Protein opsonisation is strongly linked to endocytosis mechanisms [59], and it well correlated with our experimental data showing that AuNBs are internalized by A549 cells within 24 h.

3.1.4. Cytotoxicity of uncoated AuNBs

Cytotoxicity of uncoated AuNBs was measured by HCSA [47,48,60–62] on all the chosen concentrations (2.1×10^{-12}, 5.3×10^{-12}, 1.1×10^{-11} and 1.3×10^{-11} M) as fully described in the materials and methods section. Cell count, cell membrane permeability and lysosomal mass/pH were the cell parameters monitored (Fig. 9a). In addition, quantification of the secretion of the pro-inflammatory cytokine Interleukin-6 (IL-6) was carried out for each particle size and concentration (Fig. 9b and c). A549 cells did not show any obvious reduction in cell count or any significant change in cell membrane permeability and lysosomal mass/pH when exposed to uncoated AuNBs for 24 h. It has been extensively proven that changes in the cellular membrane permeability indicate alterations of the physical condition of the cells, while a decrease or an increase of lysosomal mass/pH can be associated with an increased rate of cytotoxicity of the material tested. The secretion of IL-6 was also reduced when compared to the untreated (N/T) control, indicating that no inflammatory response was induced by exposure to uncoated AuNBs for 24 h.

3.1.5. Biodegradation of uncoated AuNBs

Evaluating the potential biochemically-induced changes of nanomaterials after administration can provide invaluable data (1) on the materials properties that are related to the observed cell responses or (2) on the potential expected responses following long-term exposure [63,64]. To assess whether uncoated AuNBs were subject to degradation following internalization into cells, $AuNB_1$ and $AuNB_2$ were retrieved from A549 cell mono-cultures by osmotic cell lysis after 24, 48 and 72 h internalization. TEM analysis showed significant changes in AuNBs morphology and wall thickness after 72 h internalization into cells, when compared to the reference, as-synthetized material (0 h) (Fig. 10a). Similarly, a significant reduction in the AuNBs size and changes in their morphology were evidenced after 72 h incubation with cells by HIM (Fig. 10b). This data was confirmed by the size distributions of AuNBs as calculated from TEM images (Fig. 10c), showing substantial reduction in AuNBs size after 72 h incubation.

In light of the extensive and comprehensive work carried out in Tier 1 to assess the biocompatibility and suitability of uncoated AuNBs as carriers, a safe-by-design approach was applied and the functionalised, multi-layered AuNBs produced were subject to a proof-of-principle testing in Tier 2 and 3.

Please cite this article in press as: Movia D, et al., A safe-by-design approach to the development of gold nanoboxes as carriers for internalization into cancer cells, Biomaterials (2014), http://dx.doi.org/10.1016/j.biomaterials.2013.12.057

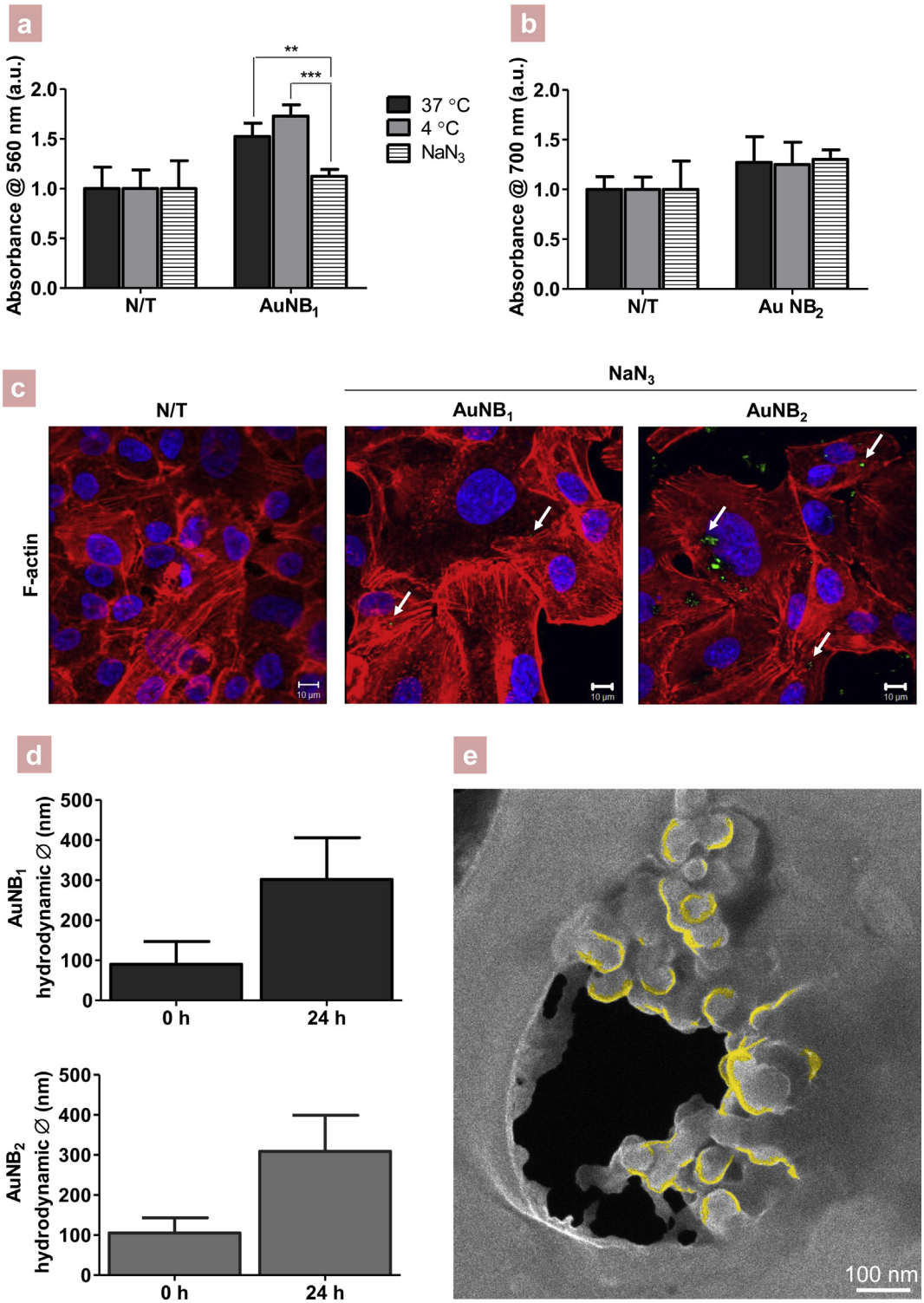

Fig. 8. (a–c) Inhibition of the internalization of uncoated AuNBs into A549 cells mono-cultures (a–b) Absorbance at (a) 560 nm and (b) 700 nm of untreated (N/T) and AuNBs-treated A549 cells. 560 nm and 700 nm are the λ_{max} of absorbance of $AuNB_1$ and $AuNB_2$, respectively. A549 cells mono-cultures were exposed to AuNBs at 37 °C (grey bars), 4 °C (light grey bars) or after pre-treatment with NaN_3 for 3 h (striped bars). Values are reported as mean ± standard deviation and are normalised on untreated controls. (c) Representative confocal images of A549 cells pre-treated with NaN_3 for 3 h. Cells were stained with rhodamine phalloidin (F-actin, in red) and Hoechst 33342 (nuclei, in blue). Uncoated AuNBs (indicated by arrows) were imaged in reflectance mode and are shown in green as pseudo-colour. Images clearly evidence that F-actin filaments maintain their overall structure as compared to an untreated (N/T) control and that uncoated AuNBs (arrows) were internalized by A549 cells even in the presence of NaN_3. (d) Changes in the hydrodynamic size (Ø) of uncoated AuNBs before (0 h) and after incubation with A549 cells for 24 h. Data are reported as mean ± standard deviation of NTA measurements. (d) Coloured HIM image of $AuNB_2$ (in yellow) after 24 h incubation with A549 cells. The AuNBs coating with biological material is evident. Scale bar: 100 nm.

Please cite this article in press as: Movia D, et al., A safe-by-design approach to the development of gold nanoboxes as carriers for internalization into cancer cells, Biomaterials (2014), http://dx.doi.org/10.1016/j.biomaterials.2013.12.057

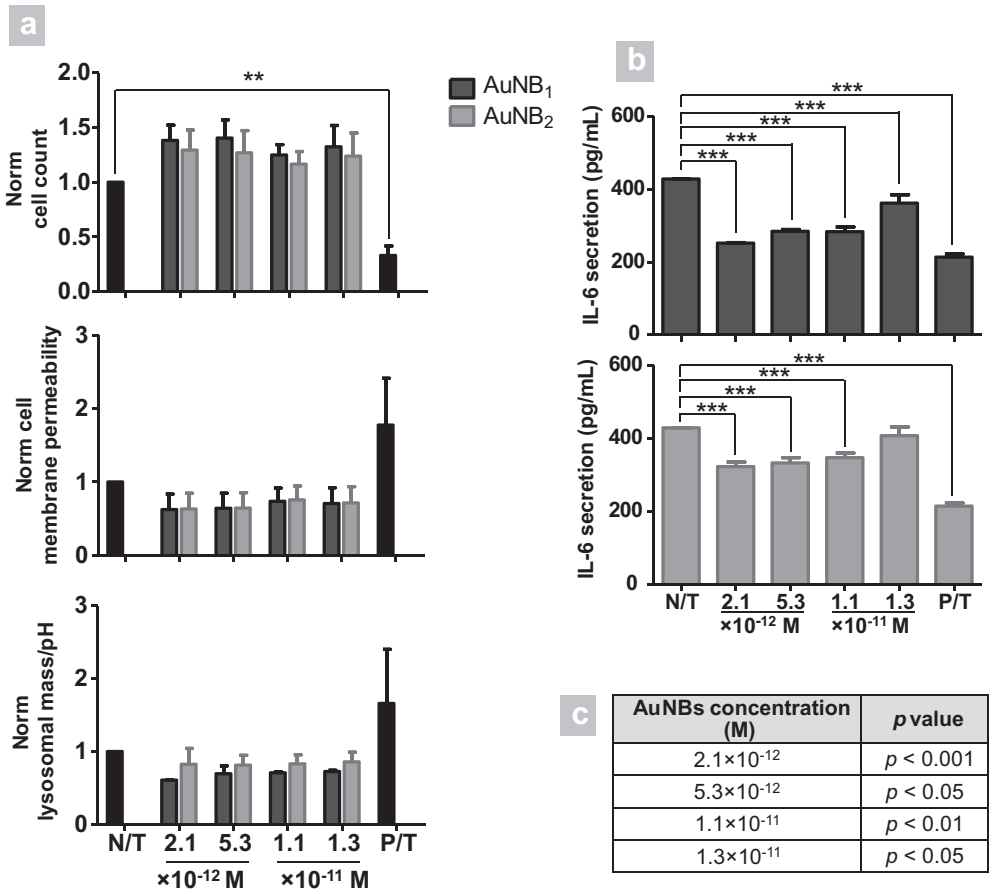

Fig. 9. Changes in the (a) cytotoxicity cell responses (cell count, cell membrane permeability and lysosomal mass/pH) and (b) IL-6 secretion from A549 cells exposed to $AuNB_1$ (black bars) or $AuNB_2$ (light grey bars) at four concentrations (2.1×10^{-12}, 5.3×10^{-12}, 1.1×10^{-11} and 1.3×10^{-11} M) for 24 h, as quantified by HCSA and ELISA respectively. Untreated and Doxorubicin-treated cells were used as negative (N/T) and positive (P/T) controls, respectively. The symbols (**) and (***) indicate significant changes ($p < 0.01$ and $p < 0.001$, respectively). Data are reported as mean ± standard deviation. (c) Statistical significance of the release of IL-6 in A549 cell cultures exposed to $AuNB_2$ as compared to the release of IL-6 in A549 cell cultures exposed to $AuNB_1$.

3.2. Tier 2

3.2.1. Biocompatibility of gelatine-coated AuNBs ($AuNB_3$)

Trypan Blue exclusion assay demonstrated that gelatin-coated AuNBs ($AuNB_3$) (Fig. 11a) did not cause any significant change in cell viability if incubated with A549 cells mono-cultures. Similarly, no significant reduction in cell viability was detectable when A549 cells were exposed to $AuNB_2$ for 24 h and 72 h (approximately 90% of live cells) (Fig. 11a), as previously shown by HCSA.

3.3. Tier 3

3.3.1. Functionalized AuNBs ($AuNB_4$ and $AuNB_5$) for drug delivery — proof-of-principle

Preliminary data showed that exposure to $AuNB_4$, $AuNB_5$ and molecular Paclitaxel (0.03 mM) caused a significant reduction in cell viability following 72 h treatment of A549 cells mono-cultures (Fig. 11b). Interestingly, folic acid-targeted AuNBs ($AuNB_5$) were more cytotoxic than the molecular drug formulation, showing a significant reduction in the percentage of live cells after 24 h and with less than 40% of live cells after 72 h exposure.

4. Discussion

A systematic qualitative and quantitative study, structured into a safe-by-design, three-tiered approach (Fig. 1), was carried out to evaluate the biological interactions of AuNBs with *in vitro* cell models representative of the human alveolar region, thus defining their potential (or, conversely, their inefficiency) as candidates for perspective translation into pre-clinical nano-enabled chemotherapeutic agents for the targeted and personalized treatment of lung cancer. Our study included systematic tests on the internalization, cytotoxicity and biodegradation of uncoated AuNBs (Tier 1), followed by preliminary testing on the drug delivery efficacy of AuNBs that underwent purpose-specific functionalization (Tier 3).

Our results showed that uncoated AuNBs were efficiently internalized by lung adenocarcinoma (A549) cells (Figs. 3 and 4) within 5–7 h (Fig. 7a) and were characterized by short-term biocompatibility, causing no detectable cytotoxic or pro-inflammatory responses in A549 cells after 24 h exposure (as assessed by cell count, cell membrane integrity, lysosomal mass/pH and IL-6 secretion) (Fig. 9). Uncoated AuNBs were detected effectively in the area corresponding to A549 cells cytoplasm by confocal microscopy (Fig. 3a), TEM (Fig. 4) and Raman spectroscopy (Fig. 3b–f), the readout signals of which are unique and could be used as fingerprints to detect AuNBs in the complex cell culture environment. We found that the cellular internalization of uncoated AuNBs in A549 cells did not decrease at 4 °C compared to the equivalent exposure at 37 °C (Fig. 8). This standard experiment [48,65] suggested that the AuNBs internalization mechanism did not involve receptor-mediated endocytosis (RME) pathways. For gold nanoparticles the RME pathways (including caveolae-mediated,

Please cite this article in press as: Movia D, et al., A safe-by-design approach to the development of gold nanoboxes as carriers for internalization into cancer cells, Biomaterials (2014), http://dx.doi.org/10.1016/j.biomaterials.2013.12.057

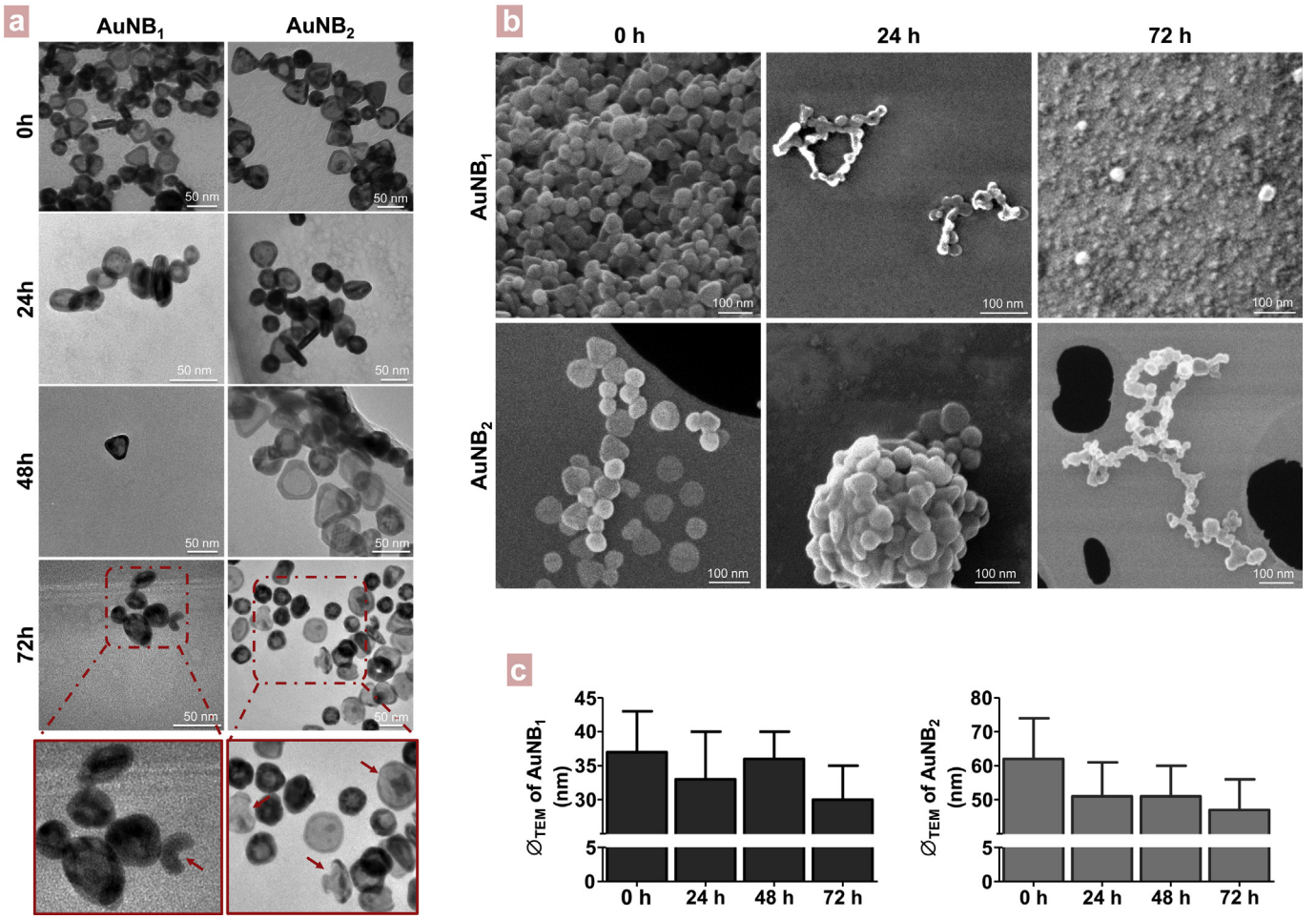

Fig. 10. (a) TEM images and (b) HIM images of flat-lying and edge-oriented uncoated AuNBs before (0 h) and after incubation with A549 cells for 24, 48 and 72 h. Arrows indicate distinct signs of AuNBs degradation. Scale bars: (a) 50 nm; (b) 100 nm. (c) Changes in the height (Ø) distribution of $AuNB_1$ (black bars) and $AuNB_2$ (grey bars) before (0 h) and after incubation with A549 cells for 24, 48 and 72 h as measured by TEM. Data are reported as mean ± standard deviation.

clathrin-mediated and caveolae/clathrin independent endocytosis) have been proposed as the primary mechanism of cellular entry [23,66–68]. However, gold nanomaterials have also been reported to be uptaken by different pathways depending on the nanomaterial size and cell type tested [69,70]. Our results showed that the internalization of $AuNB_1$ was significantly reduced in A549 cells pre-treated with 0.1% NaN_3 (Fig. 8). This suggested that the $AuNB_1$ internalization mechanism occurs through an energy-dependent process. NaN_3 is widely used *in vivo* and *in vitro* to inhibit cytochrome-C oxidase, the last enzyme in the mitochondrial electron transport chain, producing a drop in intracellular ATP concentration [48,65]. An alternative, non-RME mechanism like macropinocytosis could be therefore responsible for $AuNB_1$ internalization. To support the evidence brought in this manuscript, Gao et al. [70] showed that nanoparticles within the size range of tens to hundreds of nanometres can enter cells *via* wrapping even in the absence of clathrin or caveolin coats. In a contrasting trend, 0.1% NaN_3 did not inhibit the uptake of $AuNB_2$ in A549 cells (Fig. 8), suggesting that $AuNB_2$ enter the cells by passive transport *via* cell membrane deformation and invagination [71] as a consequence of generic physical interactions with the cells, in an action similar to the cell-penetrating peptides [59]. Further confirmation of such mechanism is provided by TEM micrographs, revealing evidence of morphological changes in the cells structure such as cell membrane invagination (Fig. 5). The *in vitro* exposure conditions, such as gravitational AuNBs sedimentation, also seemed to affect the time-dependent internalization of these nanomaterials (Fig. 7). Sedimentation of nanoparticles in cell culture is a crucial factor that should be considered when testing nanomaterials since it can affect their rate and extent of uptake *in vitro* [53], and ultimately the cell responses to the nanomaterial subject of investigation. Further research is needed to evaluate the internalization and cytotoxicity of uncoated AuNBs in A549 cells under dynamic conditions that mimic the administration of the nano-enabled drug carrier by intravenous therapy.

Despite uncoated AuNBs were also internalized into macrophage-like cell models (Fig. S4 and Fig. S6), $AuNB_1$ and $AuNB_2$ could be effectively delivered to adenocarcinoma cells in *in vitro* co-cultures of A549 and THP-1 cells (Fig. 5), suggesting that AuNBs could be used as carriers within the complex living alveolar tissue where resident phagocytic cells are present and have the main function of removing pathogens, senescent cells and external particles from the lungs [46,72,73]. Therefore, this result excluded that, in the alveolar region, macrophages could have a role in eliminating AuNBs before the nano-enabled treatment reaches the cancerogenic cellular target.

Similarly to the behaviour of other gold nanomaterials [74,75], uncoated AuNBs were successfully internalized also in 3D cell cultures mimicking the native three-dimensional architecture and microenvironment of tumours. Penetration of nanomaterials into

Please cite this article in press as: Movia D, et al., A safe-by-design approach to the development of gold nanoboxes as carriers for internalization into cancer cells, Biomaterials (2014), http://dx.doi.org/10.1016/j.biomaterials.2013.12.057

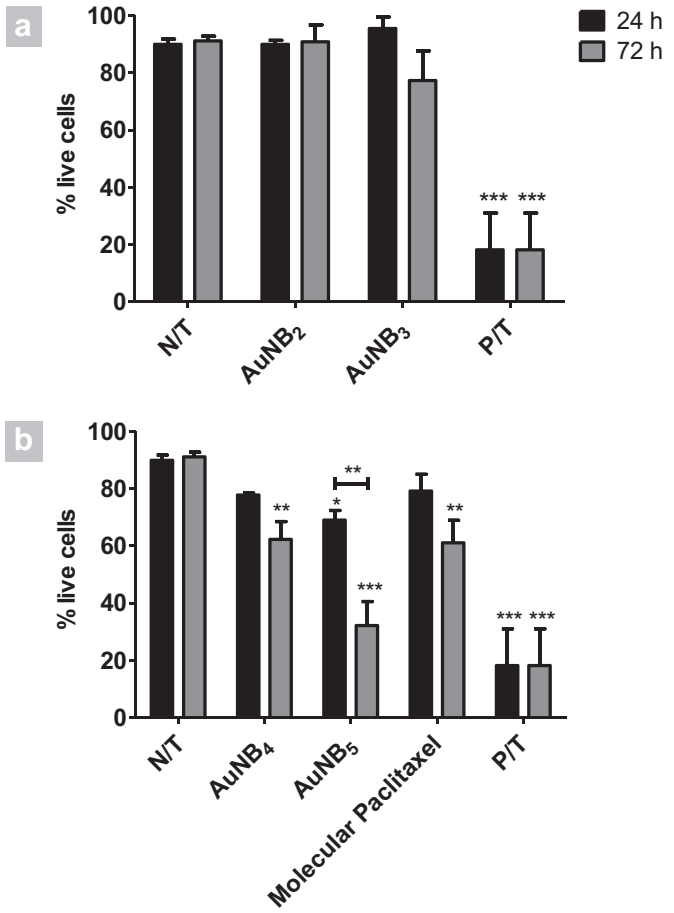

Fig. 11. Percentage (%) of live cells in A549 cells mono-cultures exposed to (a) uncoated ($AuNB_2$) and gelatine-coated ($AuNB_3$) AuNBs, or (b) functionalized ($AuNB_4$ and $AuNB_5$) AuNBs and molecular Paclitaxel, for 24 and 72 h. Untreated and methanol-treated cells were used as negative (N/T) and positive (P/T) controls, respectively. The symbols (*), (**) and (***) indicate significant changes: $p < 0.05$, $p < 0.01$ and $p < 0.001$, respectively.

the tumour environment and the tumour uptake are definitely key issues for exerting effective cancer therapy and they should not be neglected in nanomedicine studies. Since the penetration of nanomaterials in tissues is influenced by several physical factors of the particle itself [76] (e.g. particle size [77,78], hydrophobicity, hydrodynamic radius) and of the tissue microenvironment (e.g. the composition of the extracellular matrix [79]), 3D cell cultures offered a simple *ex vivo* tumour model for assessing the penetration of uncoated AuNBs of different size in a malignant tissue, and for evaluating their internalization in A549 cells in a more "*in vivo*-like" scenario. Our data indicated that uncoated AuNBs were able to reach the A549 cells by penetrating through Matrigel™ and PuraMatrix™ hydrogel layers, which ultimately reproduced the dense collagen matrix that surrounds the cancer cells *in vivo* and limits the delivery of drugs/nanomaterials to the target cells.

The final fate of uncoated AuNBs was also considered. Biopersistence of nanomaterials raises many concerns regarding the safety of nanomedicine approaches, since it may lead to impaired cell function following chronic exposure to nanomaterials [80]. The TEM and HIM results presented in this study showed that AuNBs that were internalized by A549 cells had reduced size and changed morphology after 72 h incubation (Fig. 10). This evidence suggests that AuNBs could be biodegraded by A549 cells and supports the hypothesis that uncoated AuNBs are a promising candidate as carriers for future personalised nano-enabled treatments. Further to this, TEM images showed that $AuNB_2$ internalized into A549 mono-cultures did accumulate into the lysosomes (Fig. 5c and e), which are the cellular organelles containing acid hydrolase, catabolic enzymes, thus suggesting that AuNBs degradation might happen in such cells compartment. The acidic environment of the lysosomes can in fact lead to acid etching of metallic nanoparticles, resulting in the generation of free ions from the nanoparticles surface and gradually decrease the nanoparticle core diameter [81]. However, despite biodegradation of uncoated AuNBs was evident after 72 h exposure, $AuNB_2$ did not show any detectable cytotoxicity at this exposure time (Fig. 11), suggesting that A549 cells were not affected by the free ions released by the biodegradation process.

Finally, our preliminary data showed that, while gelatin-coated AuNBs were not cytotoxic up to 72 h exposure (Fig. 11a), gelatin-coated AuNBs that were loaded with Paclitaxel ($AuNB_4$) and targeted with FA ($AuNB_5$) did cause a significant reduction in A549 cells viability after 72 h (Fig. 11b), suggesting that effective drug delivery and release to the cancer cells was achieved. Notably, exposure to $AuNB_5$ resulted in the greatest therapeutic effect as compared to $AuNB_4$ and molecular Paclitaxel, thus suggesting that FA played an important role in the efficient delivery of the nano-enabled treatment to lung cancer cells *via* interactions with FA receptors, which are over-expressed in NSCLC and can be used therefore as markers for the targeted treatment of lung cancer [82,83].

5. Conclusions

Creating an intelligent system to deliver therapeutic agents by taking advantage of targeted cell-type specificity, enhanced permeation and retention effect and reduced side-effects in physiologically healthy tissues has been the challenge of nanotechnology-based products in the last decade. In this study, we showed for the first time that uncoated AuNBs are biologically inert, can be subjected to biodegradation and can penetrate into lung cancer cells even in complex co- and 3D-culture microenvironments. Concurrently, our preliminary data on drug delivery ultimately validate our hypothesis that a safe-by-design functionalization of the AuNBs surface could produce in the future an AuNBs-based personalized medicine approach against lung cancer that delivers the drug specifically to the targeted cancer cells without affecting the surrounding healthy tissues.

Supporting data

Supplementary information is available on-line. Certain figures in this article are difficult to interpret in black and white. The full colour images can be found in the on-line version.

Authors' contribution

DM, YV and APM conceived this study, DM and APM designed the experiments and structured the paper, DM performed the biological experiments and analysed the data, carried out statistical analysis and drafted the paper. VG synthesized the AuNBs and performed their TEM characterization under YG guidance. CMM carried out NTA measurements, NJ carried out Raman spectroscopy experiments. AB carried out HIM and VN contributed to the design of the electron microscopy analysis. TT assisted and helped in the preparation of the biological specimens for TEM imaging and DS conceived the imaging of AuNBs in reflectance mode by confocal microscopy. YG contributed to reagents/materials/analysis tools. VG, CMM, NJ, AB, VN, TT, DS, YG, YV and APM revised the paper. APM finalised the paper.

Please cite this article in press as: Movia D, et al., A safe-by-design approach to the development of gold nanoboxes as carriers for internalization into cancer cells, Biomaterials (2014), http://dx.doi.org/10.1016/j.biomaterials.2013.12.057

Acknowledgements

The authors would like to acknowledge Dr. A.M. Davies (Irish National Centre for High Content Screening and Analysis) for HCSA support, the Advanced Microscopy Facility (AML) of TCD and Mr. James D.B. Gavigan-Imedio for technical support for the Trypan Blue assay. This work was supported by the EU FP7 NAMDIATREAM project (NMP-2009-LARGE-3-246479), EU FP7 MULTIFUN project (NMP-2010-LARGE-4-262943), CRANN (CRANN Pathfinder to DM) and Science Foundation Ireland (SFI) under the CRANN CSET.

Appendix A. Supplementary data

Supplementary data related to this article can be found at http://dx.doi.org/10.1016/j.biomaterials.2013.12.057.

References

[1] Weintraub K. Biomedicine: the new gold standard. Nature 2013;495:S14–6.
[2] Dreaden EC, Alkilany AM, Huang X, Murphy CJ, El-Sayed MA. The golden age: gold nanoparticles for biomedicine. Chem Soc Rev. 2012;41:2740–79.
[3] Jans H, Huo Q. Gold nanoparticle-enabled biological and chemical detection and analysis. Chem Soc Rev. 2012;41:2849–66.
[4] Schutz CA, Juillerat-Jeanneret L, Mueller H, Lynch I, Riediker M. Therapeutic nanoparticles in clinics and under clinical evaluation. Nanomed (Lond) 2013;8:449–67.
[5] Nanospectra Biosciences products: AuroLase® Therapy. Online. 2013 December. Available from: URL: http://www.nanospectra.com/clinicians/aurolasetherapy.html.
[6] Gad SC, Sharp KL, Montgomery C, Payne JD, Goodrich GP. Evaluation of the toxicity of intravenous delivery of auroshell particles (gold-silica nanoshells). Int J Toxicol 2012;31:584–94.
[7] U.S. National Institutes of Health. Online. 2013 December. Available from: URL: http://www.clinicaltrials.gov.
[8] Kumar A, Boruah BM, Liang XJ. Gold nanoparticles: promising nanomaterials for the diagnosis of cancer and HIV/AIDS. J Nanomater. http://dx.doi.org/10.1155/2011/202187. Available from: URL: http://www.hindawi.com/journals/jnm/2011/202187; 2011;2011:17. Article ID 202187.
[9] Danila D, Johnson E, Kee P. CT imaging of myocardial scars with collagen-targeting gold nanoparticles. Nanomedicine 2013;9:1067–76.
[10] Zhang L, Chang H, Hirata A, Wu H, Xue Q-K, Chen M. Nanoporous gold based optical sensor for sub-ppt detection of mercury ions. ACS Nano 2013;7:4595–600.
[11] Feng J, Zhao W, Su B, Wu J. A label-free optical sensor based on nanoporous gold arrays for the detection of oligodeoxynucleotides. Biosens Bioelectron 2011;30:21–7.
[12] Bobyk L, Edouard M, Deman P, Vautrin M, Pernet-Gallay K, Delaroche J, et al. Photoactivation of gold nanoparticles for glioma treatment. Nanomedicine 2013;9:1089–97.
[13] Niikura K, Matsunaga T, Suzuki T, Kobayashi S, Yamaguchi H, Orba Y, et al. Gold nanoparticles as a vaccine platform: influence of size and shape on immunological responses in vitro and in vivo. ACS Nano 2013;7:3926–38.
[14] Zhang XD, Wu D, Shen X, Chen J, Sun YM, Liu PX, et al. Size-dependent radiosensitization of PEG-coated gold nanoparticles for cancer radiation therapy. Biomaterials 2012;33:6408–19.
[15] Lammers T, Aime S, Hennink WE, Storm G, Kiessling F. Theranostic nanomedicine. Acc Chem Res. 2011;44:1029–38.
[16] Movia D, Poland C, Tran L, Volkov Y, Prina-Mello A. Multilayered nanoparticles for personalized medicine: translation into clinical markets. In: Bawa R, Audette GF, Rubinstein I, editors. Handbook of clinical nanomedicine: from bench to bedside 2014. Singapore.
[17] Aherne D, Gara M, Kelly JM, Gun'ko YK. From Ag nanoprisms to triangular AuAg nanoboxes. Adv Funct Mater 2010;20:1329–38.
[18] Hao E, Schatz GC. Electromagnetic fields around silver nanoparticles and dimers. J Chem Phys. 2004;120:357–66.
[19] Huber RM, Stratakis DF. Molecular oncology–perspectives in lung cancer. Lung cancer 2004;45(Suppl. 2):S209–13.
[20] Parkin DM, Bray F, Ferlay J, Pisani P. Global cancer statistics. CA Cancer J Clin 2002;2005(55):74–108.
[21] Shin D, Athanasiou K. Cytoindentation for obtaining cell biomechanical properties. J Orthop Res. 1999;17:880–90.
[22] Non-small Cell Lung Cancer Collaborative Group. Chemotherapy for non-small cell lung cancer. Cochrane Database Syst Rev 2000:CD002139.
[23] Alkilany A, Murphy C. Toxicity and cellular uptake of gold nanoparticles: what we have learned so far? J Nanopart Res. 2010;12:2313–33.
[24] Khlebtsov N, Dykman L. Biodistribution and toxicity of engineered gold nanoparticles: a review of in vitro and in vivo studies. Chem Soc Rev. 2011;40:1647–71.
[25] Cho EC, Au L, Zhang Q, Xia Y. The effects of size, shape, and surface functional group of gold nanostructures on their adsorption and internalization by cells. Small 2010;6:517–22.
[26] Alkilany AM, Nagaria PK, Hexel CR, Shaw TJ, Murphy CJ, Wyatt MD. Cellular uptake and cytotoxicity of gold nanorods: molecular origin of cytotoxicity and surface effects. Small 2009;5:701–8.
[27] Niidome T, Yamagata M, Okamoto Y, Akiyama Y, Takahashi H, Kawano T, et al. PEG-modified gold nanorods with a stealth character for in vivo applications. J Control Release 2006;114:343–7.
[28] Hauck TS, Ghazani AA, Chan WCW. Assessing the effect of surface chemistry on gold nanorod uptake, toxicity, and gene expression in mammalian cells. Small 2008;4:153–9.
[29] Alkilany AM, Nagaria PK, Wyatt MD, Murphy CJ. Cation exchange on the surface of gold nanorods with a polymerizable surfactant: polymerization, stability, and toxicity evaluation. Langmuir 2010;26:9328–33.
[30] Byrne SJ, Williams Y, Davies A, Corr SA, Rakovich A, Gun'ko YK, et al. "Jelly dots": synthesis and cytotoxicity studies of CdTe quantum dot-gelatin nanocomposites. Small 2007;3:1152–6.
[31] Aherne D, Ledwith DM, Gara M, Kelly JM. Optical properties and growth aspects of silver nanoprisms produced by a highly reproducible and rapid synthesis at room temperature. Adv Funct Mater 2008;18:2005–16.
[32] Hole P, Sillence K, Hannell C, Maguire CM, Roesslein M, Suarez G, et al. Interlaboratory comparison of size measurements on nanoparticles using nanoparticle tracking analysis (NTA). J Nanopart Res. 2013;15:2101.
[33] Gerard VA, Maguire CM, Bazou D, Gun'ko YK. Folic acid modified gelatine coated quantum dots as potential reagents for in vitro cancer diagnostics. J Nanobiotechnology 2011;9:50.
[34] Lee JH, Huh YM, Jun YW, Seo JW, Jang JT, Song HT, et al. Artificially engineered magnetic nanoparticles for ultra-sensitive molecular imaging. Nat Med 2007;13:95–9.
[35] McCarthy JR, Weissleder R. Multifunctional magnetic nanoparticles for targeted imaging and therapy. Adv Drug Deliv Rev 2008;60:1241–51.
[36] Jantzen K, Roursgaard M, Desler C, Loft S, Rasmussen LJ, Moller P. Oxidative damage to DNA by diesel exhaust particle exposure in co-cultures of human lung epithelial cells and macrophages. Mutagenesis 2012;27:693–701.
[37] Newton PE. Fundamental inhalation toxicology. In: Derelanko MJ, Hollinger MA, editors. Handbook of toxicology. 2nd ed. 2001.
[38] Kankaanpaa P, Paavolainen L, Tiitta S, Karjalainen M, Paivarinne J, Nieminen J, et al. BioImageXD: an open, general-purpose and high-throughput image-processing platform. Nat Methods 2012;9:683–9.
[39] Bazou D, Santos-Martinez MJ, Medina C, Radomski MW. Elucidation of flow-mediated tumour cell-induced platelet aggregation using an ultrasound standing wave trap. Br J Pharmacol 2011;162:1577–89.
[40] Rice WL, Van Hoek AN, Paunescu TG, Huynh C, Goetze B, Singh B, et al. High resolution helium ion scanning microscopy of the rat kidney. PLoS One 2013;8:e57051.
[41] Gérard VA. Quantum dot- and metal nanoparticle-based composites for biomedical applications. Ireland: Trinity College Dublin; 2013.
[42] DrugBank. Online. 2013 December. Available from: URL: http://www.drugbank.ca/drugs/DB01229.
[43] Caino MC, Lopez-Haber C, Kissil JL, Kazanietz MG. Non-Small cell lung carcinoma cell motility, Rac activation and metastatic dissemination are mediated by protein kinase C epsilon. PLoS ONE 2012;7:e31714.
[44] Stearns RC, Paulauskis JD, Godleski JJ. Endocytosis of ultrafine particles by A549 cells. Am J Respir Cell Mol Biol. 2001;24:108–15.
[45] Rothen-Rutishauser B, Blank F, Muhlfeld C, Gehr P. In vitro models of the human epithelial airway barrier to study the toxic potential of particulate matter. Expert Opin Drug Metab Toxicol 2008;4:1075–89.
[46] Mohamed BM, Movia D, Knyazev A, Langevin D, Davies AM, Prina-Mello A, et al. Citrullination as early-stage indicator of cell response to single-walled carbon nanotubes. Sci Rep 2013;3:1124.
[47] Mohamed BM, Verma NK, Davies AM, McGowan A, Crosbie-Staunton K, Prina-Mello A, et al. Citrullination of proteins: a common post-translational modification pathway induced by different nanoparticles in vitro and in vivo. Nanomedicine (Lond) 2012;7:1181–95.
[48] Mohamed BM, Verma NK, Prina-Mello A, Williams Y, Davies AM, Bakos G, et al. Activation of stress-related signalling pathway in human cells upon SiO_2 nanoparticles exposure as an early indicator of cytotoxicity. J Nanobiotechnology 2011;9:29.
[49] Verma NK, Conroy J, Lyons PE, Coleman J, O'Sullivan MP, Kornfeld H, et al. Autophagy induction by silver nanowires: a new aspect in the biocompatibility assessment of nanocomposite thin films. Toxicol Appl Pharmacol 2012;264:451–61.
[50] Verma NK, Crosbie-Staunton K, Satti A, Gallagher S, Ryan KB, Doody T, et al. Magnetic core-shell nanoparticles for drug delivery by nebulization. J Nanobiotechnology 2013;11:1.
[51] Blank F, Rothen-Rutishauser B, Gehr P. Dendritic cells and macrophages form a transepithelial network against foreign particulate antigens. Am J Respir Cell Mol Biol. 2007;36:669–77.
[52] Tibbitt MW, Anseth KS. Hydrogels as extracellular matrix mimics for 3D cell culture. Biotechnol Bioeng 2009;103:655–63.
[53] Cho EC, Zhang Q, Xia Y. The effect of sedimentation and diffusion on cellular uptake of gold nanoparticles. Nat Nanotechnol 2011;6:385–91.
[54] Wittmaack K. Excessive delivery of nanostructured matter to submersed cells caused by rapid gravitational settling. ACS Nano 2011;5:3766–78.

[55] Papakonstanti EA, Stournaras C. Cell responses regulated by early reorganization of actin cytoskeleton. FEBS Lett. 2008;582:2120–7.
[56] dos Santos T, Varela J, Lynch I, Salvati A, Dawson KA. Effects of transport inhibitors on the cellular uptake of carboxylated polystyrene nanoparticles in different cell lines. PLoS One 2011;6:e24438.
[57] Doorley GW, Payne CK. Cellular binding of nanoparticles in the presence of serum proteins. Chem Commun (Camb) 2011;47:466–8.
[58] Casals E, Pfaller T, Duschl A, Oostingh GJ, Puntes V. Time evolution of the nanoparticle protein corona. ACS Nano 2010;4:3623–32.
[59] Canton I, Battaglia G. Endocytosis at the nanoscale. Chem Soc Rev. 2012;41:2718–39.
[60] Movia D, Prina-Mello A, Bazou D, Del Canto E, Volkov Y, Giordani S. Screening the cytotoxicity of single-walled carbon nanotubes using novel 3D tissue-mimetic models. ACS Nano 2011;5:9278–90.
[61] Byrne F, Prina-Mello A, Whelan A, Mohamed BM, Davies A, Gun'ko YK, et al. High content analysis of the biocompatibility of nickel nanowires. J Magn Magn Mater 2009;321:1341–5.
[62] Damoiseaux R, George S, Li M, Pokhrel S, Ji Z, France B, et al. No time to lose—high throughput screening to assess nanomaterial safety. Nanoscale 2011;3:1345–60.
[63] Jenkins JT, Halaney DL, Sokolov KV, Ma LL, Shipley HJ, Mahajan S, et al. Excretion and toxicity of gold-iron nanoparticles. Nanomedicine 2013;9:356–65.
[64] Oberdorster G, Maynard A, Donaldson K, Castranova V, Fitzpatrick J, Ausman K, et al. Principles for characterizing the potential human health effects from exposure to nanomaterials: elements of a screening strategy. Part Fibre Toxicol 2005;2:8.
[65] Kim JS, Yoon TJ, Yu KN, Noh MS, Woo M, Kim BG, et al. Cellular uptake of magnetic nanoparticle is mediated through energy-dependent endocytosis in A549 cells. J Vet Sci. 2006;7:321–6.
[66] Chithrani BD, Stewart J, Allen C, Jaffray DA. Intracellular uptake, transport, and processing of nanostructures in cancer cells. Nanomedicine 2009;5:118–27.
[67] Peckys DB, de Jonge N. Visualizing gold nanoparticle uptake in live cells with liquid scanning transmission electron microscopy. Nano Lett. 2011;11:1733–8.
[68] Albanese A, Chan WC. Effect of gold nanoparticle aggregation on cell uptake and toxicity. ACS Nano 2011;5:5478–89.
[69] Wang L, Liu Y, Li W, Jiang X, Ji Y, Wu X, et al. Selective targeting of gold nanorods at the mitochondria of cancer cells: implications for cancer therapy. Nano Lett. 2011;11:772–80.
[70] Gao H, Shi W, Freund LB. Mechanics of receptor-mediated endocytosis. Proc Natl Acad Sci U S A 2005;102:9469–74.
[71] Zhao Y, Sun X, Zhang G, Trewyn BG, Slowing II , Lin VS. Interaction of mesoporous silica nanoparticles with human red blood cell membranes: size and surface effects. ACS Nano 2011;5:1366–75.
[72] Plowden J, Renshaw-Hoelscher M, Engleman C, Katz J, Sambhara S. Innate immunity in aging: impact on macrophage function. Aging Cell. 2004;3:161–7.
[73] Elkin T, Jiang X, Taylor S, Lin Y, Gu L, Yang H, et al. Immuno-carbon nanotubes and recognition of pathogens. Chembiochem 2005;6:640–3.
[74] Huo S, Ma H, Huang K, Liu J, Wei T, Jin S, et al. Superior penetration and retention behavior of 50 nm gold nanoparticles in tumors. Cancer Res. 2013;73:319–30.
[75] Huang K, Ma H, Liu J, Huo S, Kumar A, Wei T, et al. Size-dependent localization and penetration of ultrasmall gold nanoparticles in cancer cells, multicellular spheroids, and tumors in vivo. ACS Nano 2012;6:4483–93.
[76] Jain RK, Stylianopoulos T. Delivering nanomedicine to solid tumors. Nat Rev Clin Oncol 2010;7:653–64.
[77] Cabral H, Matsumoto Y, Mizuno K, Chen Q, Murakami M, Kimura M, et al. Accumulation of sub-100 nm polymeric micelles in poorly permeable tumours depends on size. Nat Nanotechnol 2011;6:815–23.
[78] Perrault SD, Walkey C, Jennings T, Fischer HC, Chan WC. Mediating tumor targeting efficiency of nanoparticles through design. Nano Lett. 2009;9:1909–15.
[79] Stylianopoulos T, Poh MZ, Insin N, Bawendi MG, Fukumura D, Munn LL, et al. Diffusion of particles in the extracellular matrix: the effect of repulsive electrostatic interactions. Biophys J 2010;99:1342–9.
[80] Sadauskas E, Danscher G, Stoltenberg M, Vogel U, Larsen A, Wallin H. Protracted elimination of gold nanoparticles from mouse liver. Nanomedicine 2009;5:162–9.
[81] Soenen SJ, Rivera-Gil P, Montenegro J-M, Parak WJ, De Smedt SC, Braeckmans K. Cellular toxicity of inorganic nanoparticles: common aspects and guidelines for improved nanotoxicity evaluation. Nano Today 2011;6:446–65.
[82] O'Shannessy DJ, Yu G, Smale R, Fu YS, Singhal S, Thiel RP, et al. Folate receptor alpha expression in lung cancer: diagnostic and prognostic significance. Oncotarget 2012;3:414–25.
[83] Nunez MI, Behrens C, Woods DM, Lin H, Suraokar M, Kadara H, et al. High expression of folate receptor alpha in lung cancer correlates with adenocarcinoma histology and EGFR [corrected] mutation. J Thorac Oncol 2012;7:833–40.

Please cite this article in press as: Movia D, et al., A safe-by-design approach to the development of gold nanoboxes as carriers for internalization into cancer cells, Biomaterials (2014), http://dx.doi.org/10.1016/j.biomaterials.2013.12.057